THE DYNAMICS OF THE LATE NEOGENE ANTARCTIC ICE SHEETS IN THE CENTRAL ROSS SEA USING A MULTIANALYTICAL APPROACH

Christopher Wallace Mallery

Submitted to the faculty of the University Graduate School
in partial fulfillment of the requirements
for the degree
Master of Science
in the Department of Earth Sciences,
Indiana University

June 2022

Accepted by the Graduate Faculty of Indiana University, in partial fulfillment of the requirements for the degree of Master of Science.

Master's Thesis Committee

_____
Kathy Licht, PhD, Chair

_____
Catherine Macris, PhD

_____
William Gilhooly III, PhD

DEDICATION

For Scarlett and Amy.

ACKNOWLEDGEMENT

In appreciation of the faculty and staff of the Earth Science Department at IUPUI for all of the great help and support over the years. With acknowledgements to my contemporaries in the earth sciences programs and the lab group individuals for their support and help including Tori, Sarah, and Conner for their work on the zircon samples. Gratitude to the University of Arizona Laserchron, especially Stuart for work on the zircons. Cheers and thanks to Tina and Jim for their neodymium isotope work and Matteo and Luca for their clast lithology work. Acknowledgements to the NSF, grant NSF PLR-1443342, and IODP Leg 374 scientists and crew. Thank you to my graduate committee, Kathy, Cam, and Bill for hanging in there for me! Extra praise to Kathy for allowing me in on this project and for the inexhaustible list of things she's done, without which this would not have been possible.

Christopher Wallace Mallery

THE DYNAMICS OF THE LATE NEOGENE ANTARCTIC ICE SHEETS IN THE CENTRAL ROSS SEA USING A MULTIANALYTICAL APPROACH

With the goal of determining ice sheet history in the central Ross Sea since the late Miocene, the provenance of glacial till from IODP expedition 374 site U1522 was assessed using a suite of three analyses. A total of 3,869 zircons, between 250-63 microns in size, from sixteen different cores were measured for U-Pb isotopes via LA-ICP-MS. Zircon data was compared to neodymium isotope and clast lithology datasets from collaborators. Site U1522 shows three distinct provenance shifts from the late Miocene to the Pleistocene, two of which are coincident with Ross Sea Unconformities three and two. Late Miocene samples have abundant Cretaceous zircon populations, radiogenic neodymium values, and clasts interpreted as having a West Antarctic provenance. In latest Miocene samples, zircons are mostly Ross Orogeny age (c. 470-615 Ma) and Cretaceous zircon grains are almost absent, neodymium values are relatively un-radiogenic, and dolerite clasts are present signaling a shift to East Antarctic derived ice. Above Ross Sea Unconformity 3, early to mid-Pliocene samples show a shift back to West Antarctic provenance with abundant Cretaceous zircons and more radiogenic neodymium values. Late Pliocene to Pleistocene samples, deposited above Ross Sea Unconformity 2, reflect dominant East Antarctic provenance with few Cretaceous zircon dates, relatively un-radiogenic neodymium values, and the presence of dolerite clasts. These data are broadly in agreement with ice sheet interpretations suggested by clast analysis from ANDRILL site AND-1B.

Permo-Triassic zircon dates suggest the presence of unexposed bedrock of this age beneath the West Antarctic Ice Sheet based on their association with Cretaceous dates that have not been reported from East Antarctica. The zircon dataset also reveals two late Miocene intervals with a previously undocumented Eocene-Oligocene magmatic event ~30-40 Ma. The coexistence of Cretaceous dates in these intervals suggests a likely West Antarctic source. The absence of Eocene-Oligocene zircons in subsequent Plio-Pleistocene sediments may be explained by substantial erosion and offshore deposition of the West Antarctic interior, including volcanic edifices following the Middle Miocene Climatic Transition.

Kathy Licht, PhD, Chair

Catherine Macris, PhD

William Gilhooly III, PhD

TABLE OF CONTENTS

LIST OF TABLES

LIST OF FIGURES

LIST OF ABBREVIATIONS

- AND-1B - ANDRILL Site 1B
- AND-2A - ANDRILL Site 2A
- ANDRILL - Antarctic Drilling Project
- ANDRILL 1B - Antarctic Drilling Project Site 1B
- ANDRILL 2A - Antarctic Drilling Project Site 2A
- DSDP - Deep Sea Drilling Project
- EA - East Antarctica
- εNd - Epsilon Neodymium
- IODP - International Ocean Discovery Program
- μm - Microns/Micrometers
- REMA - Reference Elevation Model Antarctica
- SAL(s) xxxx - Sediment Analysis Lab Sample(s) XXXX
- U-Pb - Uranium Lead
- WA - West Antarctica
- WAIS - West Antarctic Ice Sheet

INTRODUCTION

Sectors of the Antarctic Ice Sheets that are grounded below sea level are more susceptible to oceanic forcings (i.e. circumpolar deep-water intrusion) which are influenced by average global temperatures (Mercer, 1978; Rignot et al., 2019). Large volumes of the ice sheet grounded in West Antarctica reside on a bed that is well below sea level whereas the bed in East Antarctica, with exceptions, is primarily above or very near sea level (Figure 1-B) (Fretwell et al., 2013). Modern projections predict increasing mass loss of land-based ice concordant with rising global mean surface air temperature and that the marine grounded West Antarctic Ice Sheet could be one of the larger contributors to increases in sea level through the end of the century (Edwards et al., 2021). However, uncertainty exists in the Antarctic response to such scenarios (Edwards et al., 2021). Degradation and abrupt loss of ice shelves (e.g. the Ross Ice Shelf), which offer a buttressing effect on the ice sheet, are suggested as a major contributing factor to rapid increased mass loss from West Antarctica (Mercer, 1978; Rignot et al., 2019; Edwards et al., 2021). The volume of water stored in grounded West Antarctic ice is equivalent to approximately 5.3 meters in sea level (Rignot et al., 2019). Melt or ungrounding (i.e. floating) of a high percentage of that volume would inundate low-lying coastal areas and displace populations that reside nearby.

The greatest uncertainty in sea level rise predictions is the future of the Antarctica ice sheet, particularly the West Antarctic Ice Sheet (WAIS), and the study of past ice sheet dynamics is important for inferring ice sheet dynamics of the future (Mercer, 1978). The history of Antarctic ice in the Ross Embayment comes from continental shelf-wide ice sheet overriding events including grounded WAIS expansion beginning in the early

Miocene (Marschalek et al., 2021). Glacigenic sequences through the Miocene have been observed at Antarctic Drilling Project (ANDRILL) sites located on the far western side of the Ross catchment near Ross Island (Figure 1-A) (McKay et al., 2012; McKay et al., 2017; McKay et al., 2018). These provide detailed records of ice margin fluctuations through that time. However, their location is not ideal for reconstructing fluctuations of the WAIS because of their proximity to East Antarctica (Figure 1-A). Deep Sea Drilling Project (DSDP) sites 270-272 located on the central-eastern Ross continental shelf were preferably located for interpreting WAIS dynamics since the late Miocene, but had very poor core recovery through that interval (Figure 1-A & D) (McKay et al., 2018). This data gap prompted International Ocean Discovery Program (IODP) Expedition 374. Sediments recovered from IODP site U1521 (Figure 1-A) record West Antarctic dominated ice sheet overriding events in the early Miocene but have a limited record of tills younger than the middle Miocene (McKay et al., 2019[b]; Marschalek et al., 2021). IODP site U1522, located on the central Ross Sea continental shelf recovered late Miocene-Pleistocene glacial tills. It can fill gaps in the sediment record at a prime location that captures ice derived from both East and West Antarctica and thereby inform ice sheet provenance through this period (Figures 1 & 2).

A method to accomplish the goal of evaluating past fluctuations of the WAIS is zircon provenance analysis of Ross Sea glacial tills (e.g. McKay et al., 2012; Licht et al., 2014). Zircon U-Pb isotopes can be used to characterize the distribution of crystallization dates for zircons from various core intervals of site U1522. These dates can then be compared with published zircon U-Pb dates for bedrock and glacial till sources in the Ross Sea catchment. Thereby, the origin for the till of a given interval or series of cores

and whether it was deposited primarily by East Antarctic or West Antarctic derived ice may be inferred. In this study, 3869 zircon dates from sixteen till samples from site U1522 were combined with a suite of other provenance proxies to determine whether ice advances onto the central Ross Sea continental shelf since the late Miocene were dominated by ice derived from the East or West Antarctic ice sheet.

SETTING - LOCATION & MODERN CONDITIONS

The Ross Sea catchment drains approximately one third of Antarctica, including ice from both the East and West Antarctic ice sheets, onto the Ross continental shelf (Figure 1-C) (Rignot et al., 2019). The WAIS moves ice from deep in its interior into the Ross Embayment in relatively fast flowing ice streams, whereas East Antarctic ice flows much more slowly from the continental interior until it reaches outlet glaciers crossing the Transantarctic Mountains (Rignot et al., 2019) (Figure 1-C). IODP site U1522 is located on the central Ross continental shelf edge and is near the convergence between ice derived from both East and West Antarctica during the last glacial maximum (Licht et al., 2014) (Figures 1-A & 2).

The elevation of Antarctica's ice-bed interface differs between East and West Antarctica. Much of West Antarctica is below sea level and much of its lowest topography is in its interior (Fretwell et al., 2013) (Figure 1-B). In contrast, much of East Antarctica is above sea level where many of its topographically lowest regions are around its edges (e.g. the Wilkes Subglacial Basin) (Fretwell et al., 2013; Paxman et al., 2019) (Figure 1-B). This is important to the dynamics of how the ice sheets in these different sectors may respond to climatic forcings including warm water intrusion and ice shelf collapse (i.e. Mercer, 1978). Marine based ice sheets with ice shelves are more vulnerable to oceanic and atmospheric warming and the loss of the Ross and Ronne-Filchner ice shelves would initiate rapid degradation of the marine based WAIS (Mercer, 1978).

Antarctica's bedrock topography in the Ross Sea catchment has been modified by glaciers over time. Model reconstructions indicate a substantial reduction in elevation of the West Antarctic interior since the Eocene-Oligocene boundary, concomitant with

increases in thickness and seaward extent on the central Ross continental shelf from sediment deposition (Paxman et al., 2019) (Figure 3). These areas where glacial till has accumulated are settings that harbor the glacial history of Antarctica.

Bedrock and glacial moraine till outcrops in the Ross Sea catchment are seen primarily amid the Transantarctic Mountains of East Antarctica and the Marie Byrd Land Dome of West Antarctica (Figure 4). Rock and till outcrops in the Ross Sea catchment are the best (only) example of the lithologies available for erosion onto the Ross Sea continental shelf, as most of Antarctica is covered in ice. Therefore, these are used for comparison with the glacial tills deposited in the Ross Sea during past ice advances. The components of glacial till sequences deposited in the Ross Sea reflect an amalgamation of what was eroded and entrained along the ice flow path. However, it is possible that terrains yet to be identified currently remain covered by ice sheets and their presence is suggested from their chronological fingerprints and unique lithologies found in glacial tills (e.g. Perotti et al., 2017; Licht et al., 2018).

Overview of relevant geologic history

Antarctica has an extensive geologic history, its rock record spanning ~3.5 Ga (Harley et al., 2013). The East Antarctic craton has been involved in supercontinental amalgamations as early as the Mesoproterozoic whereas the West Antarctic microcontinents were (likely) accreted to East Antarctica during the Cambrian assemblage of Gondwana (Dalziel, 2013; Harley et al., 2013). Some of those formative events are recorded in zircons that now reside in Ross Sea continental shelf sediments, transported offshore by ice. Zircon U-Pb dates from rock outcrops, glacial moraines, and

ice stream tills around the Ross Sea were compiled and plotted as histograms to illustrate the distribution of zircon dates from the different sectors of Antarctica (Figure 5).

Rifting of the supercontinent Rodinia was initiated in the Neoproterozoic (c. ~750 Ma) after which a passive rift margin formed between Laurentia and Antarctica (Dalziel, 2013; Elliot, 2013). This was followed by the development of the Cambrian active margin responsible for the Ross Orogen and emplacement of granites ~550-480 Ma (Elliot, 2013) (e.g. the Granite Harbor Intrusives) (Figure 5). The sediments produced during the passive rifting of Rodinia and from the Ross Orogeny contributed detritus into a growing foreland basin on the margin of the East Antarctic craton (Goodge et al., 2012; Elliot, 2013). These deposits form the rocks of the Beacon Supergroup and are now exposed in the Transantarctic Mountains. The Beacon Supergroup contains extensive Devonian-Jurassic rock sequences composed largely of sandstones and mudstones. Zircons from these sedimentary sequences show shifts in paleoflow and detrital inputs (Elliot et al., 2017). The lower formations of the Beacon Supergroup are dominated by zircon U-Pb age peaks ~580 Ma and the upper formations contain large populations with age peaks ~500 Ma and ~245 Ma (Elliot et al., 2017) (Figure 5). They are intruded by dolerite sills and basaltic pyroclastic flood lavas of the Ferrar Large Igneous Province emplaced rapidly between ~182.8-182.6 Ma (Elliot, 2013; Elliot & Fleming, 2018) during the initiation of Gondwana rifting (Figure 5).

Cambro-Ordovician turbidites and flysch derived in part from the Ross Orogen and deposited along the Gondwanide margin make up what is now the metasedimentary Swanson Formation exposed in West Antarctica (Jordan et al., 2020). The Swanson Formation was intruded by the Devonian-Carboniferous Ford Granodiorite (c. 358-336

Ma) and the Cretaceous Byrd Coast Granite (c. 115-98 Ma) associated with continental arc activity and continental rifting respectively (Korhonen et al., 2009) (Figure 5). Surges of granitoid magmatism and metamorphism associated with the active continental margin of East Gondwana throughout the Paleozoic-Triassic are recorded in rock units of the Fosdick Migmatite-Granite Complex and other western Marie Byrd Land metasediments (Jordan et al., 2020; Korhonen et al., 2009; Yakymchuk et al., 2015).

The rifting of Gondwana that commenced in the early Jurassic marked the initiation of the West Antarctic Rift System (Elliot, 1992; Bialas et al., 2007). The most rapid extension occurred between ~105 Ma and ~90 Ma during the late Cretaceous producing zircon-bearing igneous intrusions (e.g., the Byrd Coast Granite) (Bialas et al., 2007; Siddoway, 2007) (Figure 5). During this period of relatively quick crustal extension, the Ross Sea Embayment widened substantially (Wilson et al., 2012) forming the area now covered by the West Antarctic Ice Sheet. Cenozoic volcanism associated with late phases of the West Antarctic Rift System has continued scattered throughout this area (e.g., LeMasurier, 1990; Rocci et al., 2005).

The geologic history of Antarctica is also reflected in the neodymium isotopic values of bedrock sources, glacial tills, and in sediments that have been deposited on the Ross Sea continental shelf (e.g. Farmer & Licht, 2016; Marschalek et al., 2021) (Figure 6). Neodymium analysis of till is performed on the <63 μm size fraction, which reflect the homogenized value of source rocks eroded. Less radiogenic (more negative) neodymium values reflect mixtures of lithologies present in the Transantarctic Mountains of East Antarctica whereas more radiogenic (more positive) values better reflect mixtures of West Antarctic bedrock (Farmer et al., 2006; Farmer & Licht, 2016; Marschalek et al.,

2021) (Figure 6). Therefore, the neodymium value of a till/sediment of unknown provenance is suggestive of its origin.

BACKGROUND - ICE SHEET HISTORY

Inception of ephemeral, though perhaps continental scale ice sheets in Antarctica began at the Eocene-Oligocene boundary ~34 Ma (Zachos et al., 1992; Gasson et al., 2016; Pollard & DeConto, 2020). Topographic reconstructions of Antarctica suggest extensive landscape evolution since the Oligocene especially in West Antarctica. This involved erosion of the bed throughout the West Antarctic continental interior and sediment deposition on the Ross Sea continental shelf (Paxman et al., 2019) (Figure 3). Reconstructions imply that despite the relatively warm Oligocene climate, West Antarctica had sufficient topography above sea level to nucleate ephemeral ice caps (Zachos et al., 2001; Paxman et al., 2019). Lithostratigraphic and sedimentological changes seen in early through mid-Miocene sediments deposited at ANDRILL site 2A (AND-2A) also suggest large scale fluctuations in the Antarctic Ice Sheet margin, possibly heavily affected by bed topography (Fielding et al., 2011; Gasson et al., 2016). Bed topography played and continues to play an intrinsic role in the dynamics and stability of the Antarctic Ice Sheets especially in West Antarctica (Gasson et al., 2016; Paxman et al., 2019).

Simulations suggest grounding excursions of the WAIS on the continental shelf edge in the early Miocene (Pollard & DeConto, 2020). This is supported by recent provenance evidence from IODP site U1521 which indicates WAIS grounding on the central Ross continental shelf ~17.8 Ma (Marschalek et al., 2021). Seismic reflection data compared with lithologic and biostratigraphic descriptions from DSDP Leg 28 sites (e.g., Figure 1-A) suggest that glacial erosion features and unconformities (Ross Sea Unconformities) are associated with ice advances since the Oligocene through the early

Miocene (DeSantis et al., 2013; McKay et al., 2019[a]). Numerous grounded ice advance and retreat cycles also are evident in the late Miocene through the Pleistocene sequence recovered from ANDRILL site 1B (AND-1B) on the far western Ross continental shelf (McKay et al., 2009; Rosenblume & Powell, 2019). A primary objective of coring at site U1522 was to date ice sheet advances associated with Ross Sea Unconformities 3 and 2, identify the origin of advancing ice, and determine whether those correspond to overriding events observed at AND-1B (McKay et al., 2019[a]).

The benchmark glacial record of Antarctic Ice Sheet history in the Ross Sea through the late Miocene is considered to be AND-1B. It is suggested that since ice derived from East Antarctica grounded here (several hundred meters below sea level), this site reflects the overall state of the marine based ice sheet in the Ross Embayment (McKay et al., 2012). McKay et al. (2012) also imply that the collapse of grounded ice over AND-1B would have also required partial to complete collapse of the WAIS. DSDP Leg 28 sites 270-272 had poor/little recovery for the late Miocene interval (McKay et al., 2018). Most ice overriding site AND-1B was derived from East Antarctica via the adjacent Transantarctic Mountains and therefore may not be an accurate analogue for WAIS dynamics in the late Miocene.

Accurate interpretation of the history of the Antarctic Ice Sheets in the Ross Sea back through the late Miocene requires characterization of tills deposited by ice derived from both East and West Antarctica. Knowledge of where East and West Antarctic ice converge is key to this depiction. Last glacial maximum flow reconstructions have been created by utilizing the very fine sand sized zircons from glacial tills as provenance tracers (Licht et al., 2014) (Figure 2). Licht et al. (2014) suggest convergence between

East and West Antarctic derived ice occurred between ~170-180° West on the central Ross Sea continental shelf during the last glacial maximum (Figure 2). This indicates that the late Miocene-Pleistocene history of both the East and West Antarctic Ice Sheets may be preserved in glacial tills at site U1522 and that provenance studies of these tills may better characterize ice sheet dynamics for the whole Ross Sea than tills from AND-1B.

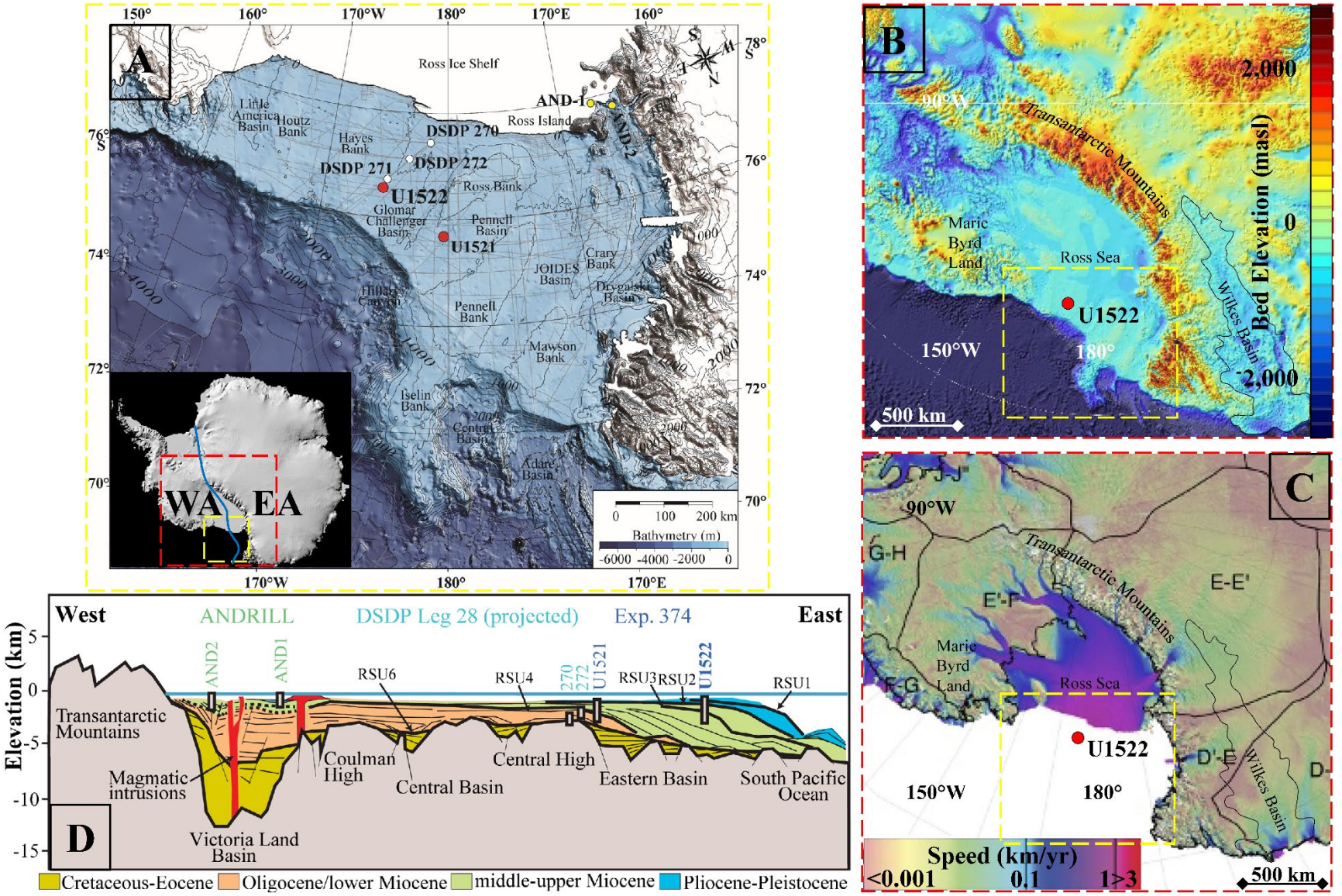
A
Ross Ice Shelf
AND-1
Ross Island
AND-2
DSDP 270
DSDP 271
DSDP 272
U1522
U1521
Ross Bank
Little America Basin
Houtz Bank
Hayes Bank
Glomar Challenger Basin
Pennell Basin
Crary Bank
JOIDES Basin
Drygalski Basin
Hillary Canyon
Pennell Bank
Mawson Bank
Iselin Bank
Central Basin
Adare Basin
WA
EA
0 100 200 km
Bathymetry (m)
-6000 -4000 -2000 0
150°
160°
170°W
180°
170°E
76°S
74°
72°
70°
78°S
B
2,000
0
-2,000
Bed Elevation (masl)
90°W
Transantarctic Mountains
Marie Byrd Land
Ross Sea
Wilkes Basin
U1522
150°W
180°
500 km
C
90°W
G-H
E-E'
E'-F'
Transantarctic Mountains
Marie Byrd Land
F-G
Ross Sea
U1522
D'-E'
D-
Wilkes Basin
150°W
180°
Speed (km/yr)
<0.001
0.1
1>3
500 km
D
West
ANDRILL
DSDP Leg 28 (projected)
Exp. 374
East
Elevation (km)
5
0
-5
-10
-15
AND2
AND1
RSU6
RSU4
270
272
U1521
RSU3
RSU2
U1522
RSU1
Transantarctic Mountains
Magmatic intrusions
Victoria Land Basin
Coulman High
Central Basin
Central High
Eastern Basin
South Pacific Ocean
Cretaceous-Eocene
Oligocene/lower Miocene
middle-upper Miocene
Pliocene-Pleistocene

Figure 1. **Ross Sea catchment and continental shelf maps**

A: Bathymetric map of the Ross Sea continental shelf (modified from McKay et al., 2018) with inset of the Reference Elevation Model of Antarctica (REMA) (modified from Howat et al., 2019). The solid blue line on the REMA map indicates the approximate tectonic delineation between West Antarctica (WA) and East Antarctica (EA) (Tinto et al., 2019). The dotted yellow and red rectangles on the REMA map indicate the approximate area of the bed elevation map (B) and ice velocity map (C). B: Modern bed elevation of the Ross Sea catchment (modified from Fretwell et al., 2013). C: Modern ice velocity and flow divides of the Ross Sea catchment (note that not all area shown drains into the Ross Sea e.g. J-J") (modified from Rignot et al., 2019). D: Illustrated seismic cross section of several glacial till packages on the Ross Sea continental shelf including Ross Sea Unconformities (RSU) and previous drilling expeditions ANDRILL and DSDP (modified from McKay et al., 2018). Till depositional intervals are differentiated by color. Spatial context between (A) and (D) is provided by the locations of AND-1(B)/AND-2(A), DSDP 270-272, and IODP U1521/U1522.

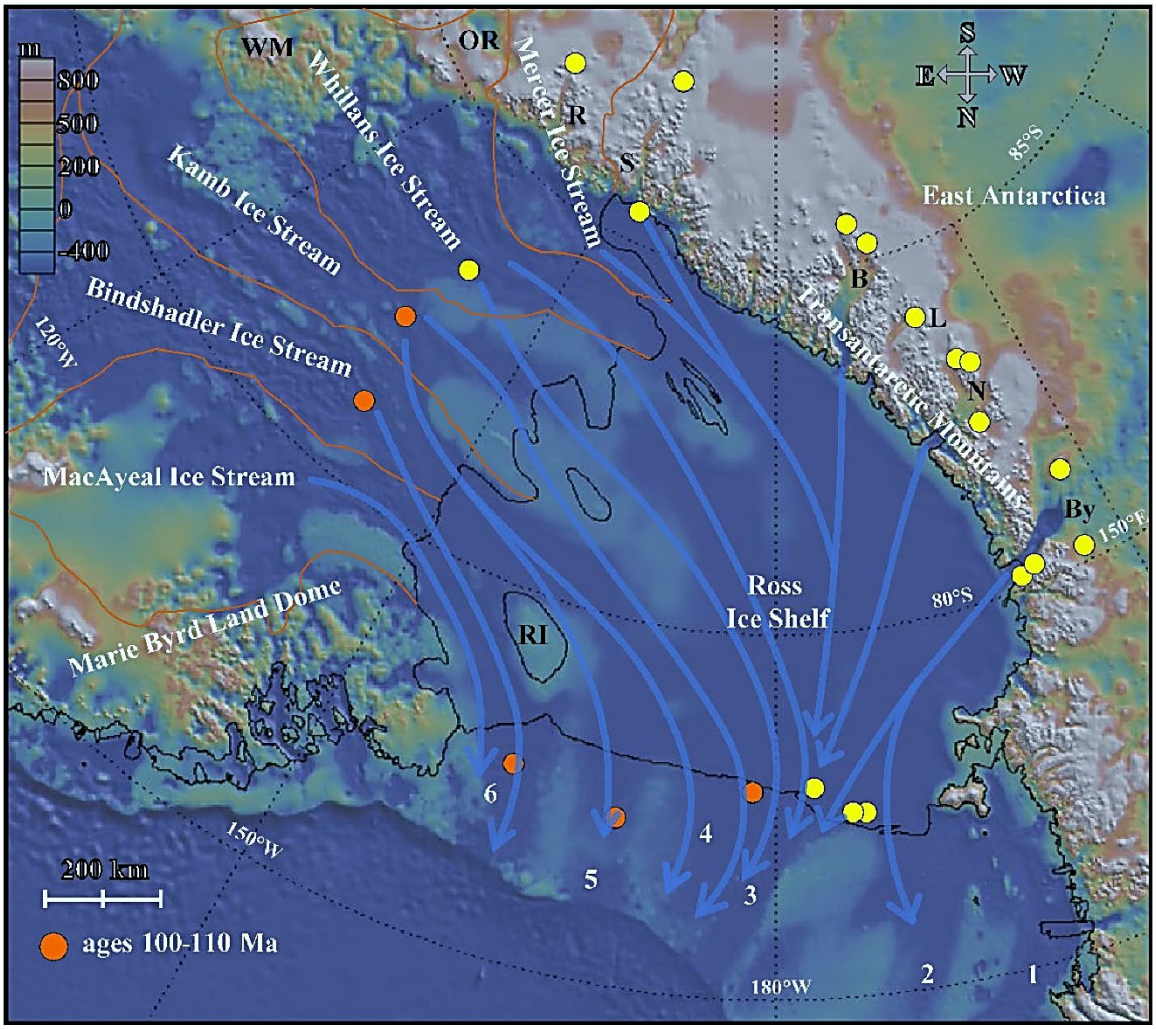

Figure 2. **Last glacial maximum ice flow reconstruction for the Ross Sea**

Orange and yellow dots indicate locations of samples where detrital zircons were dated using U-Pb isotopes. Samples shown with orange dots contained Cretaceous dates and were found only in Kamb and Bindschadler Ice Streams and in glacial tills east of 180° longitude. Abbreviations include: B = Beardmore Glacier, By = Byrd Glacier, L = Law Glacier, N = Nimrod Glacier, OR = Ohio Range, R = Reedy Glacier, S = Scott Glacier, WM = Whitmore Mountains, and numerals 1-6 are sea floor troughs labeled according to Mosola & Anderson, 2006. Modified from Licht et al., 2014.

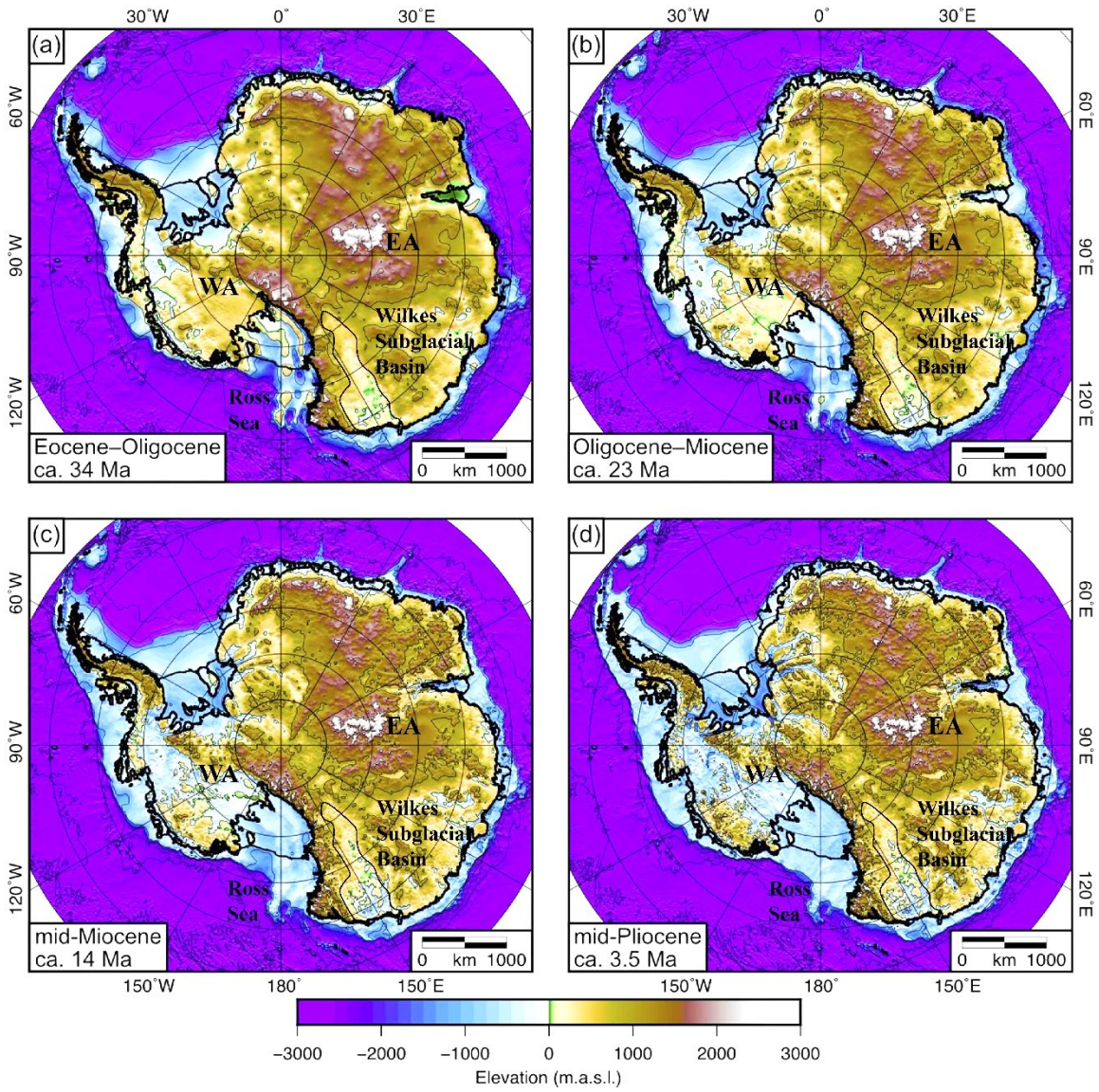

Figure 3. **Reconstructed topographic maps of Antarctica**

Maps show four time slices since approximately the Eocene-Oligocene (E-O) boundary. Large topographic changes occurred in the Ross Sea catchment of West Antarctica (WA) since the E-O boundary. Most erosion in East Antarctica in the Ross Sea catchment occurred primarily through outlet glaciers in the Transantarctic Mountains and the Wilkes Subglacial Basin. Modified from Paxman et al., 2019.

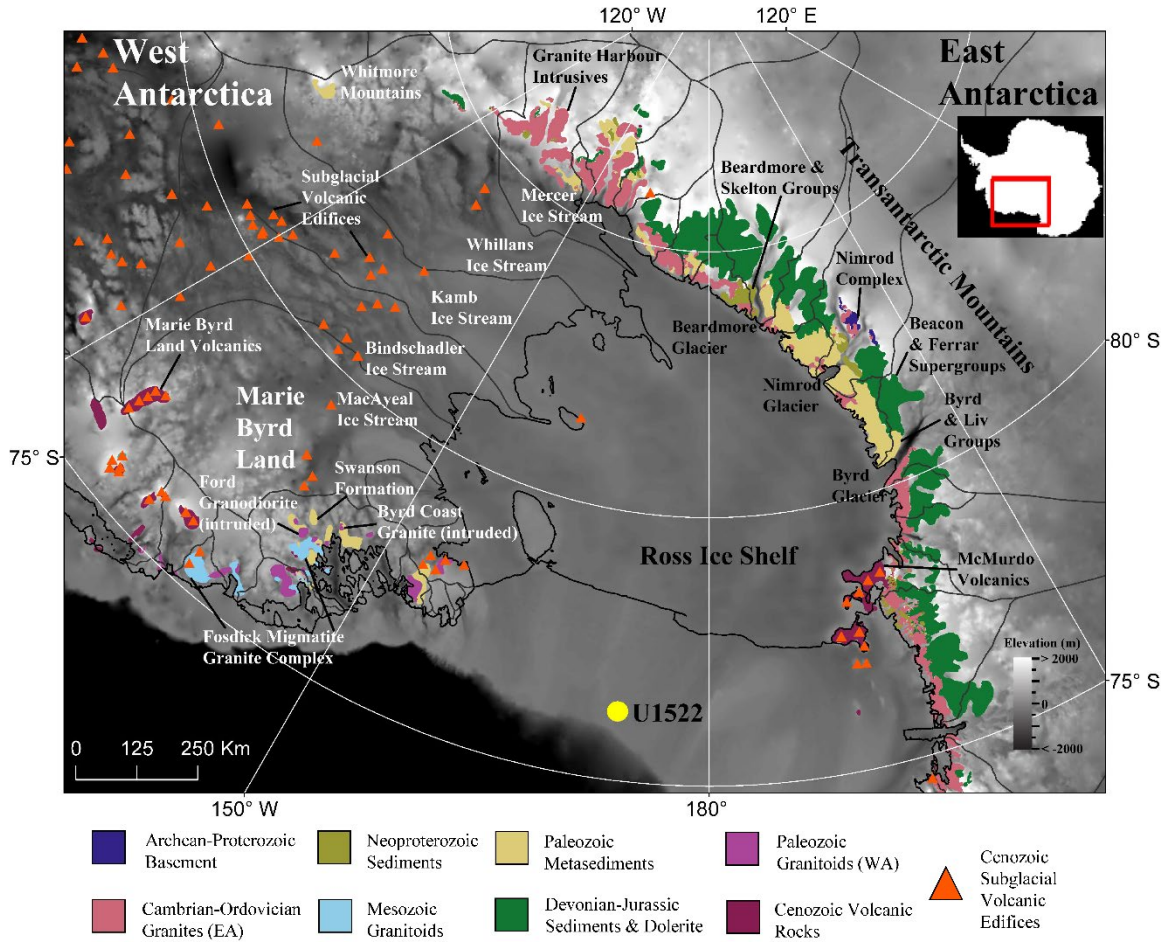

Figure 4. **Regional bedrock geology around the Ross Sea catchment**

Rocks of Archean to Cenozoic age crop out in the Transantarctic Mountains of East Antarctica. The most common units include the Cambro-Ordovician Byrd Group, the Cambro-Ordovician Granite Harbor Intrusives, the Devonian-Jurassic Beacon Supergroup, and the Jurassic Ferrar Dolerite. Rock units in West Antarctica's Ross Sea catchment range from early Paleozoic to Cenozoic in age and are exemplified by lithologies seen in Marie Byrd Land including the Cambrian Swanson Formation, the late Devonian-early Carboniferous Ford Granodiorite, and the Cretaceous Byrd Coast Granite. Byrd Coast Granite and Ford Granodiorite units are not individually colored as they are intruded throughout the Swanson Formation metasedimentary outcrops.

Mesoproterozoic to Neoproterozoic rocks occur in the Whitmore Mountains among younger Cambro-Ordovician units. Three major East Antarctic outlet glaciers that drain through the Transantarctic Mountains into the Ross Sea are labeled near their mouths. West Antarctic Ice Streams that feed into the Ross Sea are labeled along the Siple Coast. Zircon dates within geologic units are not necessarily limited to their depositional age (e.g. recycled Cambro-Ordovician and Precambrian zircons are prevalent in the Devonian-Jurassic cover units of the Beacon Supergroup in the Transantarctic Mountains). Modified from Marschalek et al., 2021.

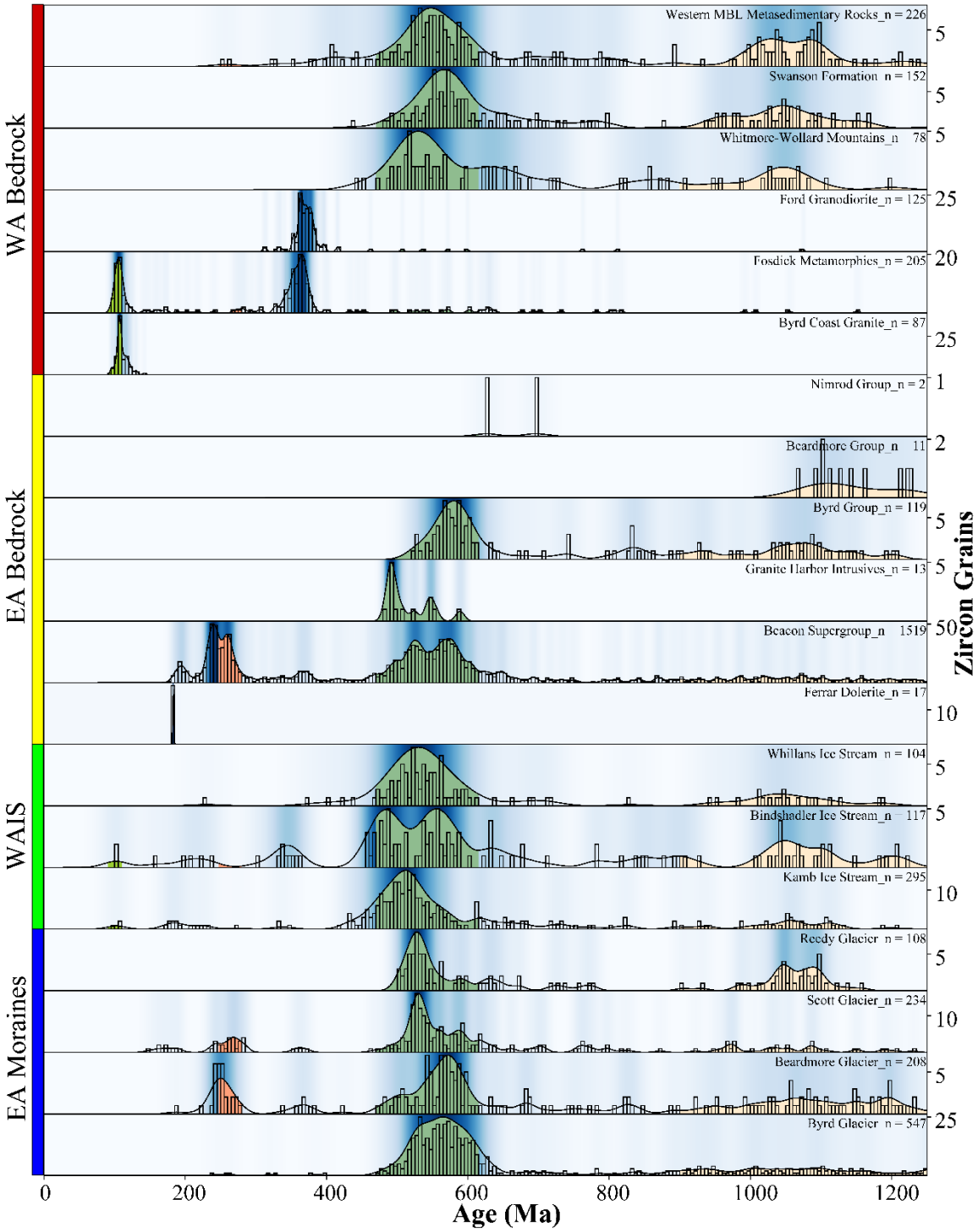

Figure 5. **Compilation of U-Pb dates from sources around the Ross Sea**

Sources include East and West Antarctic bedrock, West Antarctic ice stream till, and East Antarctic glacial moraine till. Histograms are overlain with kernel density

estimates that are colored for different zircon producing events which include Cretaceous volcanism (c. 90-110 Ma), the Gondwanide Orogeny (c. 247-280 Ma), the Ross Orogeny (c. 470-615 Ma), and the Grenville Orogeny (c. 900-1,300 Ma) (green, salmon, forest green, and beige respectively). Heat maps shown in blue on each histogram indicate the density of zircons at given dates where more saturated tones reflect more dates. Not all units have a similar number of analyses, nor do they necessarily reflect the overall volume of these rock units in the region. The total number of zircons shown for each unit (n) appears next to each unit name. Colored bars on the left y-axis highlight different sources. WAIS = West Antarctic Ice Streams, WA = West Antarctica, EA = East Antarctica.

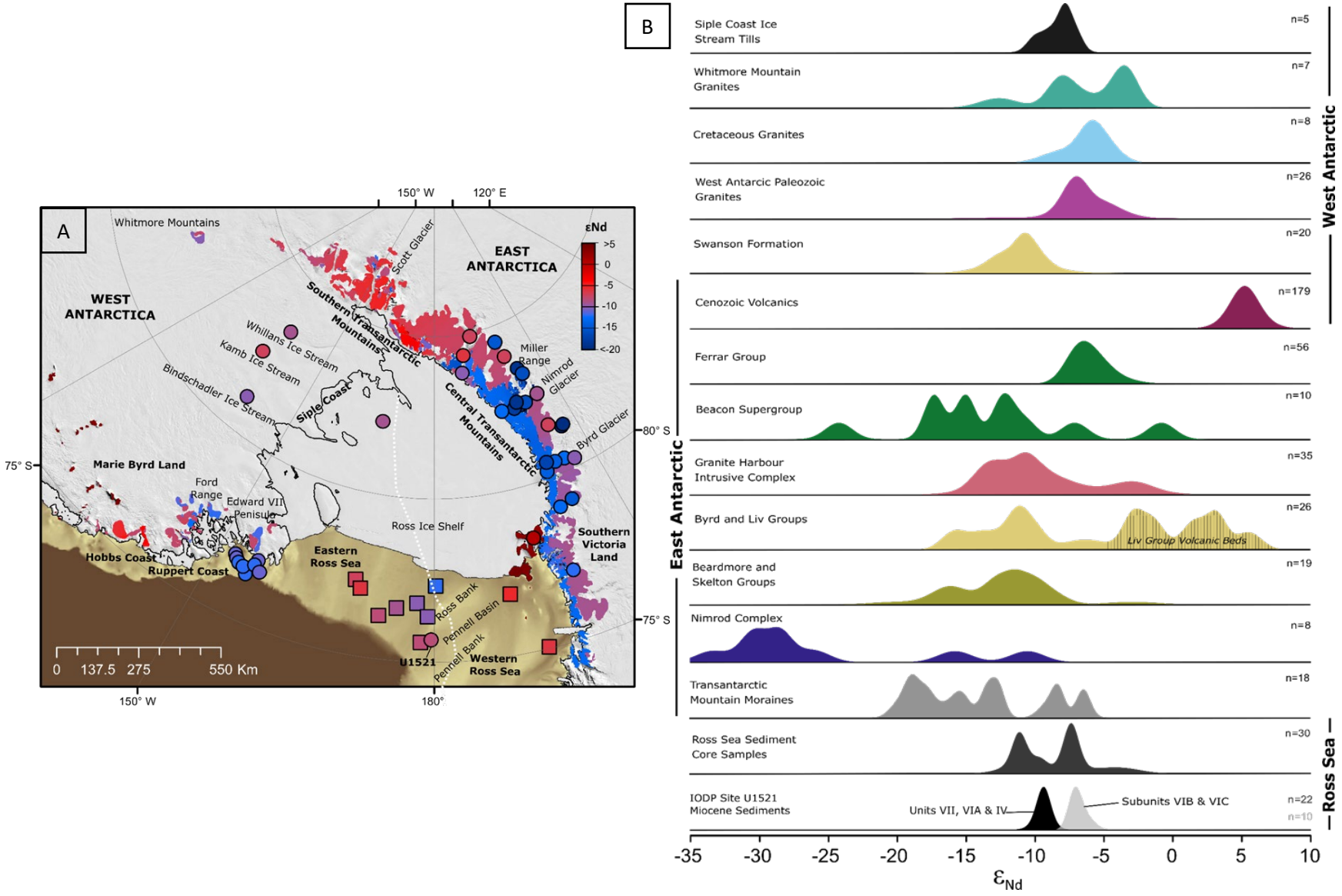
A
Whitmore Mountains
WEST ANTARCTICA
EAST ANTARCTICA
Scott Glacier
Southern Transantarctic Mountains
Whillans Ice Stream
Kamb Ice Stream
Bindschadler Ice Stream
Siple Coast
Miller Range
Nimrod Glacier
Central Transantarctic Mountains
Byrd Glacier
εNd
>5
0
-5
-10
-15
<-20
150° W
120° E
75° S
80° S
Marie Byrd Land
Ford Range
Edward VII Peninsula
Ross Ice Shelf
Southern Victoria Land
Hobbs Coast
Ruppert Coast
Eastern Ross Sea
Ross Bank
Pennell Basin
Pennell Bank
U1521
Western Ross Sea
0 137.5 275 550 Km
150° W
180°
B
Siple Coast Ice Stream Tills
n=5
Whitmore Mountain Granites
n=7
Cretaceous Granites
n=8
West Antarctic Paleozoic Granites
n=26
Swanson Formation
n=20
Cenozoic Volcanics
n=179
Ferrar Group
n=56
Beacon Supergroup
n=10
Granite Harbour Intrusive Complex
n=35
Byrd and Liv Groups
n=26
Liv Group Volcanic Beds
Beardmore and Skelton Groups
n=19
Nimrod Complex
n=8
Transantarctic Mountain Moraines
n=18
Ross Sea Sediment Core Samples
n=30
IODP Site U1521 Miocene Sediments
Units VII, VIA & IV
Subunits VIB & VIC
n=22
n=10
East Antarctic
West Antarctic
Ross Sea
-35 -30 -25 -20 -15 -10 -5 0 5 10
εNd

Figure 6. **Neodymium isotope values (εNd) around the Ross Sea catchment**

A: Map of εNd from ice stream and glacial moraine tills, offshore sediments, and bedrock sources around the Ross Sea. Circles and squares show εNd for late Quaternary tills and color mapping shows regional bedrock εNd. The white dotted line represents the lithospheric boundary between East and West Antarctica (Tinto et al., 2019). B: Kernel density estimate plots of εNd for ice stream tills, offshore sediments, and bedrock sources around the Ross Sea. Together the map and kernel density estimate plots show that the least radiogenic (most negative) εNd values occur in East Antarctic sources and that average εNd values are more radiogenic (more positive) for West versus East Antarctic sources. Modified from Marschalek et al., 2021.

METHODS

IODP site U1522 is a single rotary bored hole cored to 701.8 meters below the seafloor and is located in the Glomar Challenger Basin at 76°33.2262′S, 174°45.4652′W, 557.60 meters below sea level (McKay et al., 2019[a]) (Figures 1-A & 7). Sediments from U1522 are dominantly massive diamictite interpreted to be glacigenic and were deposited from the late Miocene ~11 Ma through the last glacial maximum in the late Pleistocene ~26.5-19 ka (McKay et al., 2019[a]; Anderson et al., 2014) (Figure 7). Drilling recovered 279.57 meters of sediment that is divided into four lithostratigraphic units which were defined by several features including diamict lithification, sharp contacts indicated by changes in clast size/distribution, and sharp contacts indicated by color and lithology changes (McKay et al., 2019[a]) (Figure 7).

Detrital zircon grains of sixteen core samples from different depths of site U1522 were analyzed for U-Pb isotopes via laser ablation single collector inductively coupled plasma mass spectrometry (Table 1). Sand sized zircon grains between 250 microns (μm) and 63 μm were isolated from the samples via physical and chemical disaggregation techniques, sieving, magnetic separation, and heavy liquid separation.

Samples were prepared in two batches. The first batch consisted of ten samples which were coarsely broken into approximately medium pebble to sand sized clumps. They were then freeze dried to help un-clump the clays, put in test tubes with a 20% sodium metaphosphate to 80% deionized water solution, mixed in a vortex and sonicated for ten minutes before being left to soak overnight in the sodium metaphosphate and deionized water solution. The following morning, they were mixed and sonicated to resuspend the sediments prior to sieving. Due to the difficult and time-consuming

disaggregation, a different method was used on the second batch, which was effective. The second batch consisted of six samples which were coarsely broken-down like the first batch and then soaked for a minimum 20 days in beakers with an 85% to 15% solution of dimethyl sulfoxide and distilled water (Triplehorn et al., 2002). Batch two samples were periodically stirred and further disaggregated with pressure into mostly sand size particles while soaking. All samples were wet sieved stepwise with 250 μm and 63 μm sieves to isolate the fine to very fine sand fractions for comparison to previously published data (e.g. Figure 5). Sand sized aggregates remaining after wet sieving were broken apart manually with a pick under a microscope and suspended in deionized water with a sonicating probe, re-sieved using a 63 μm sieve, and examined under a microscope to ensure the sample separates consisted only of clean, individual mineral grains. All samples were dried in an oven and then transferred into glass jars with a funnel and brush. All sieves and tools were cleaned in between different samples in a sonicator and with picks if necessary.

Ten of the sixteen samples were magnetically separated by the Argon Geochronology for the Earth Sciences Lab at Columbia University's Lamont Doherty Earth Observatory and the other six by the University of Arizona's Laserchron Center and ZirChron LLC. Magnetic separation was performed by hand magnet and with a Frantz LB1 Barrier Field Magnetic Separator. This process was performed after sieving and sorted the 63-250 μm sand separates into ferromagnetic and paramagnetic mineral fractions. After magnetic separation, heavy liquid separation was performed by the Arizona Laserchron Center and ZirChron LLC via the 'popsicle' technique using

diiodomethane (methylene iodide - MI/MEI, 3.32 g/cm^3) (Gehrels et al., 2008) to further isolate zircons.

Minerals remaining after the previous steps were poured through an ~1/2 inch inside diameter aluminum cylinder onto double sided tape adhered to a white ceramic plate and individually picked with fine tweezers under a microscope to remove residual pyrite grains. Loose sample grains were pressed into the tape with tweezers and zircon standards were mounted next to the samples. Zircon standards FC-1, SL2, and R33 were used (Paces & Miller, 1999; Black et al., 2004; Gehrels et al., 2008; Mattinson, 2010). One inch inside diameter plastic rings were positioned over the sample grains on the tape and were filled with Buehler Epo-Thin clear epoxy. The epoxy was left to solidify ~24 hours inside the ring forms, creating pucks containing the samples and standards. The pucks were removed from the ceramic plates, polished ~1/3 of the way into the zircon grains with 2500 grit sandpaper to create a uniform flat surface, and backscatter electron imaged on a scanning electron microscope so individual zircon grains could be identified.

Uranium and lead isotopes were analyzed on a Thermo Fischer Element 2 single collector inductively coupled plasma mass spectrometer. Zircon grains were ablated with an analyte G2 excimer laser producing an ~30 µm diameter by ~15 µm deep laser pit (Gehrels et al., 2006). Ideally 200-300 zircon grains were ablated for each sample to maximize the probability of capturing small age populations (Pullen et al., 2014; Vermeesch and Garzanti, 2015). Best age measurements were determined with $^{206}Pb/^{238}U$ isotopes for analyses with ages less than 900 Ma and with $^{206}Pb/^{207}Pb$ isotopes for analyses with ages greater than 900 Ma.

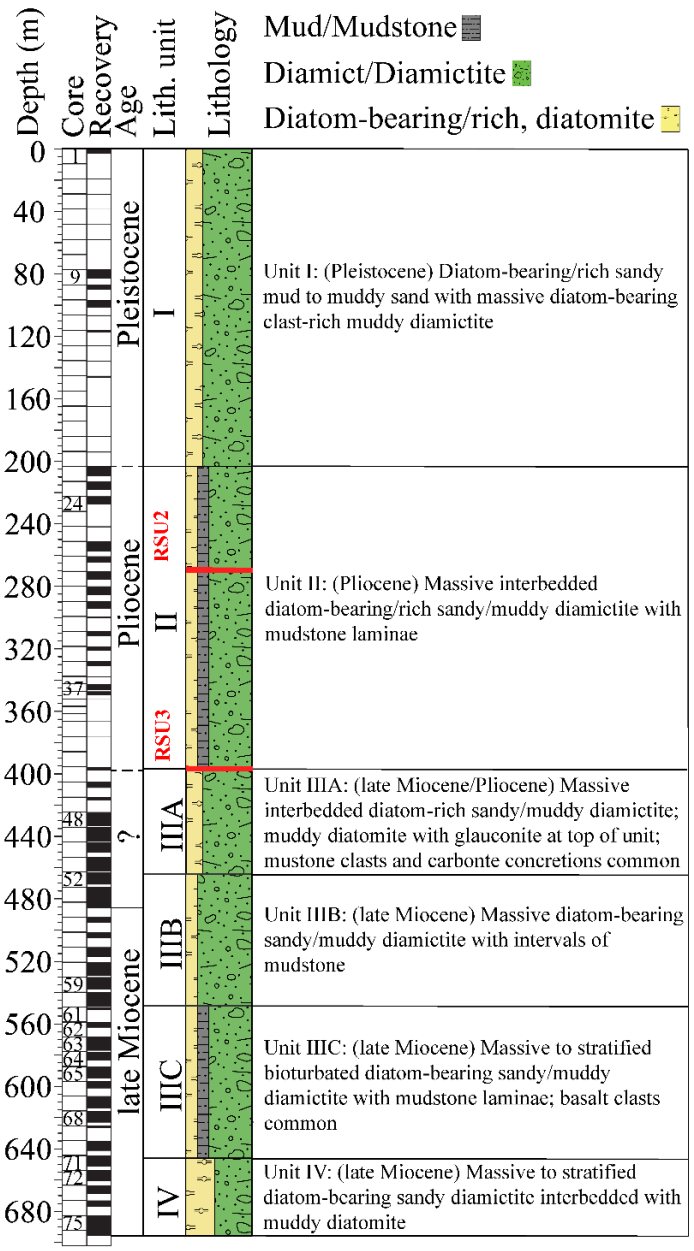

Figure 7. **Lithostratigraphic summary of site U1522**

The sixteen cores sampled in this study are labeled by number in their respective boxes in the *Core* column. Approximate percent recovery of each core is shown by the degree of shading beside it. Approximate locations of Ross Sea Unconformities are shown with red lines on the lithology log. Modified from McKay et al., 2019[a].

Table 1. Sample information for zircon analysis of site U1522 tills.

Sample Number (SAL)	Core Type - Section	Top Depth (m)	Bottom Depth (m)	Length (cm)	Volume (cm3)	Sample Type	Zircons Analyzed (n)
2285	1R-2	2.12	2.42	30	250	QRND	158
2286	9R-2	79.1	79.5	40	250	QRND	306
2287	24R-3	226.4	226.8	40	250	QRND	291
2288	37R-2	344	344.5	50	250	QRND	254
2289	48R-3	427.62	428.02	40	250	QRND	301
2290	52R-3	466.13	466.53	40	250	QRND	302
2291	59R-4	533.99	534.39	40	250	QRND	229
2316	61R-CC	550.57	550.79	22	150	QRND	192
2317	62R-2	560.02	560.24	22	150	QRND	274
2292	63R-3	571.55	571.95	40	250	QRND	222
2318	64R-4	582.09	582.31	22	150	QRND	237
2319	65R-1	587.3	587.41	11	150	HRND	161
2293	68R-3	619.22	619.62	40	250	QRND	250
2320	71R-4	648.4	648.51	11	150	HRND	142
2321	72R-1	653.94	654.05	11	150	HRND	246
2294	75R-3	686.11	686.51	40	250	QRND	304

R = rotary bore
CC = core catcher
QRND = quarter-round
HRND = half-round
n = total number of zircons dates

ZIRCON U-Pb RESULTS

A total of 3869 U-Pb dates from detrital zircons are reported in this analysis of site U1522; they ranged in age from ca. 31 Ma to 3605 Ma (Appendix A). In all of the samples, greater than ca. 91% of the zircon dates are younger than 1250 Ma. All the samples have age peaks coincident with regional zircon producing events but in differing relative abundances (Figure 8). Throughout the samples, the most abundant dates are associated with the Ross Orogeny (c. 615-470 Ma), with the exception of SAL 2288. The second most abundant zircon population includes dates younger than the Gondwanide Orogeny (c. 280-247 Ma) with the exceptions of SAL 2289 and SAL 2290. The least abundant populations of zircons occur in the Grenville Orogeny (c. 1,300-900 Ma) with the exceptions of SALs 2285, 2286 and 2287 whose Grenville dates outnumber those younger than the Gondwanide Orogeny. All the samples contain some Cretaceous zircons, but their relative numbers vary by sample and core interval.

The sixteen samples from site U1522 can be grouped by similarities in their zircon signatures. The relative proportions of Grenville, Ross, Triassic-Jurassic, and Cretaceous-age zircons in the lowest ten samples deposited during the late Miocene are generally similar (Figure 8). The exceptions within this group are SAL 2294 and SAL 2292. SAL 2294 contains 10 zircons younger than 40 Ma (c. 33.2 Ma peak); SAL 2292 contains 47 zircons younger than 40 Ma (ca. 34 Ma peak) indicating significant input from an Oligocene source. Above these ten samples, SALs 2290 and 2289, deposited during the latest Miocene, have very similar zircon signatures dominated by Ross-age peaks and to a lesser extent Grenville-age zircons. Mesozoic zircons are relatively few in these samples. SAL 2288, deposited during the Pliocene, contains a high proportion of

Triassic-Jurassic age zircons compared to its number of dates falling within the Ross Orogeny. It also has a relatively large proportion of Cretaceous-age grains and lower numbers of Grenville zircons compared to the samples above and below. The uppermost three samples, SALs 2287, 2286, and 2285, deposited in the latest Pliocene to the late Pleistocene respectively, contain similar proportions of Ross, Grenville, and Cretaceous zircons, and to a lesser extent Triassic-Jurassic age zircons. SAL 2287 has the most Mesozoic dates among these three samples.

Multi-dimensional scaling plots were made for the detrital zircon samples from site U1522 to quantitatively compare their similarity/dissimilarity and identify which samples might have been derived from similar parent populations (Figure 9). Samples plot as points in Cartesian coordinates where samples nearer one another are more similar (i.e., have a higher degree of similarity between their cumulative distribution functions or probability density plots depending on the comparison criterion) and samples distant from one another are dissimilar (Vermeesch, 2013; Saylor & Sundell, 2016; Nordsvan et al., 2020) (Figure 9). The two-sample Kolmogorov-Smirnov and Kuiper tests use different statistics to evaluate the similarity/dissimilarity between samples. The Kolmogorov-Smirnov test D statistic is more sensitive to dissimilarity between the medians of different cumulative distribution functions (Vermeesch, 2013) compared to the Kuiper test V statistic, which has equal sensitivity for the entire cumulative distribution functions of different samples, including the tails of the data (Saylor & Sundell, 2016). Cross-Correlation of probability density plots evaluates the degree of similarity between samples (i.e., the presence/absence of age peaks, and changes in their shapes and magnitude) by calculating the coefficient of determination (R^2 value) for their

cross plots, where samples with a higher degree of similarity have an R^2 value nearer to 1 and samples with a lower degree of similarity have an R^2 value nearer to 0 (Saylor & Sundell, 2016).

The three multi-dimensional scaling approaches named here associate the detrital zircon samples from site U1522 into three conspicuous groups that contain between two and five samples. Three samples are outliers (SALs 2288, 2292, and 2294) (Figure 9). All three multi-dimensional scaling plots (Figure 9) group SALs 2289 and 2290 nearby one another but isolated from all other samples. However, whereas SALs 2288 and 2292 are distant from the other samples, SAL 2294 is in moderate proximity to two of the groups in the Kolmogorov-Smirnov and Kuiper plots. SALs 2293 and 2320 show the widest degree of variation when compared by the different metrics; their spatial relationship appears to widen modestly between the Kolmogorov-Smirnov and Kuiper comparisons and substantially by the Cross-Correlation comparison. Cross-Correlation amplifies the separation between samples that also appear isolated when plotted using the Kolmogorov-Smirnov and Kuiper tests.

SALs 2285, 2286, 2287, 2316, 2317, and 2319 plot nearby each other in all tests; however, their spatial relationship is closer on the Kolmogorov-Smirnov and Kuiper plots (Figure 9). SAL 2318 joins this group on the Cross-Correlation plot. SALs 2291, 2293, 2318, 2320, and 2321 group near each other on both the Kolmogorov-Smirnov and Kuiper plots, but their spread is wider on the Kuiper plot. In the Cross-Correlation plot, SALs 2291, 2293, 2320, and 2321 group nearby one another albeit more distantly than they do in either the Kolmogorov-Smirnov or Kuiper plots.

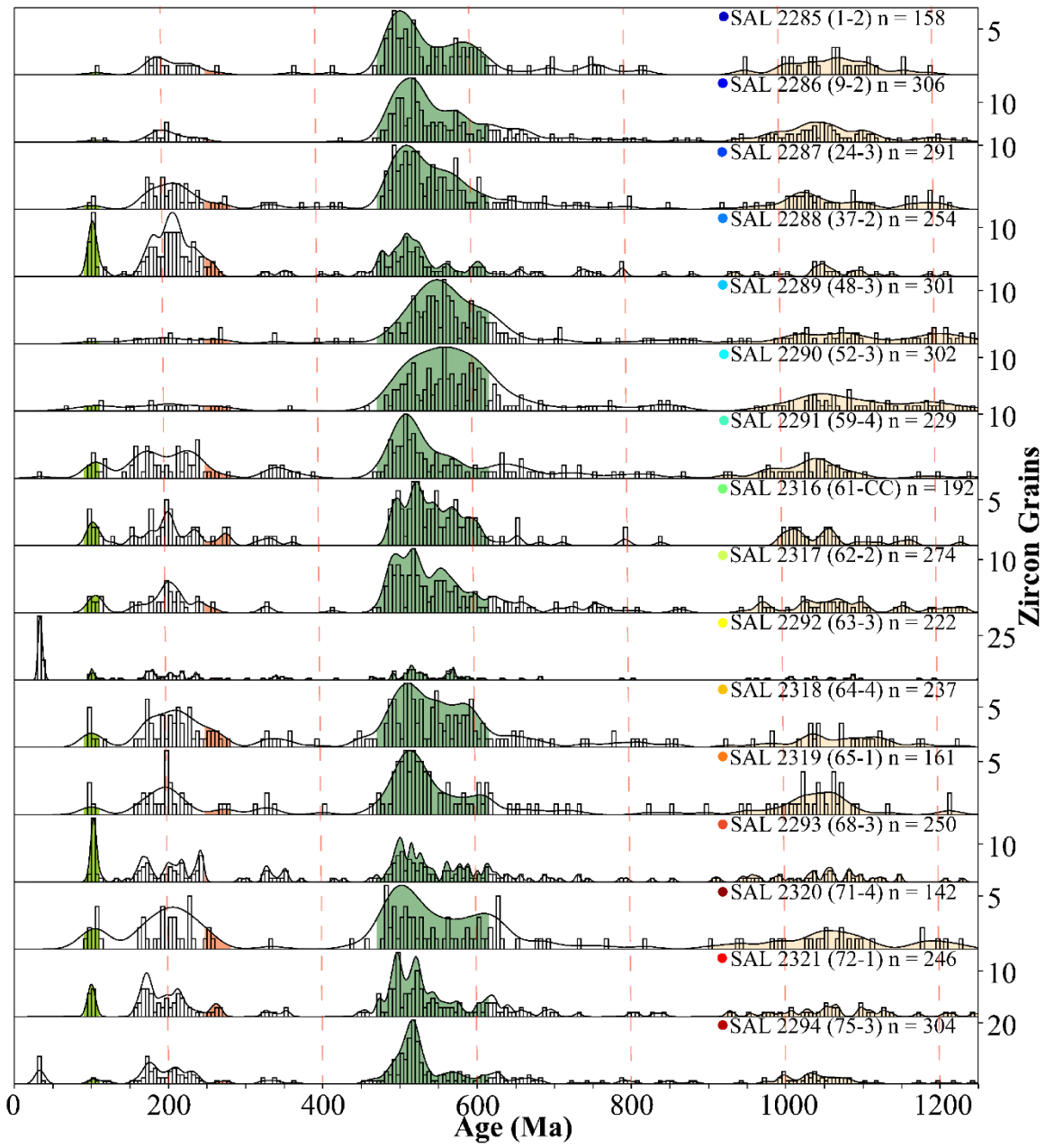

Figure 8. **Detrital zircon U-Pb dates from sixteen site U1522 core samples**

Samples are plotted as histograms overlain with kernel density estimates. Samples are arranged in stratigraphic order, the lowest (i.e. SAL 2294) being furthest below the sea floor. Colored areas under the kernel density estimates highlight zircon producing events including Cretaceous volcanism (c. 90-110 Ma), the Gondwanide Orogeny (c.

247-280 Ma), the Ross Orogeny (c. 470-615 Ma), and the Grenville Orogeny (c. 900-1,300 Ma) (green, salmon, forest green, and beige respectively). Individual samples are labeled in the upper right corner of each histogram with the total number of zircon grains (n) analyzed per sample. Colored dots beside the sample labels are unique to each sample and match the colors of the sample dots in figures that follow.

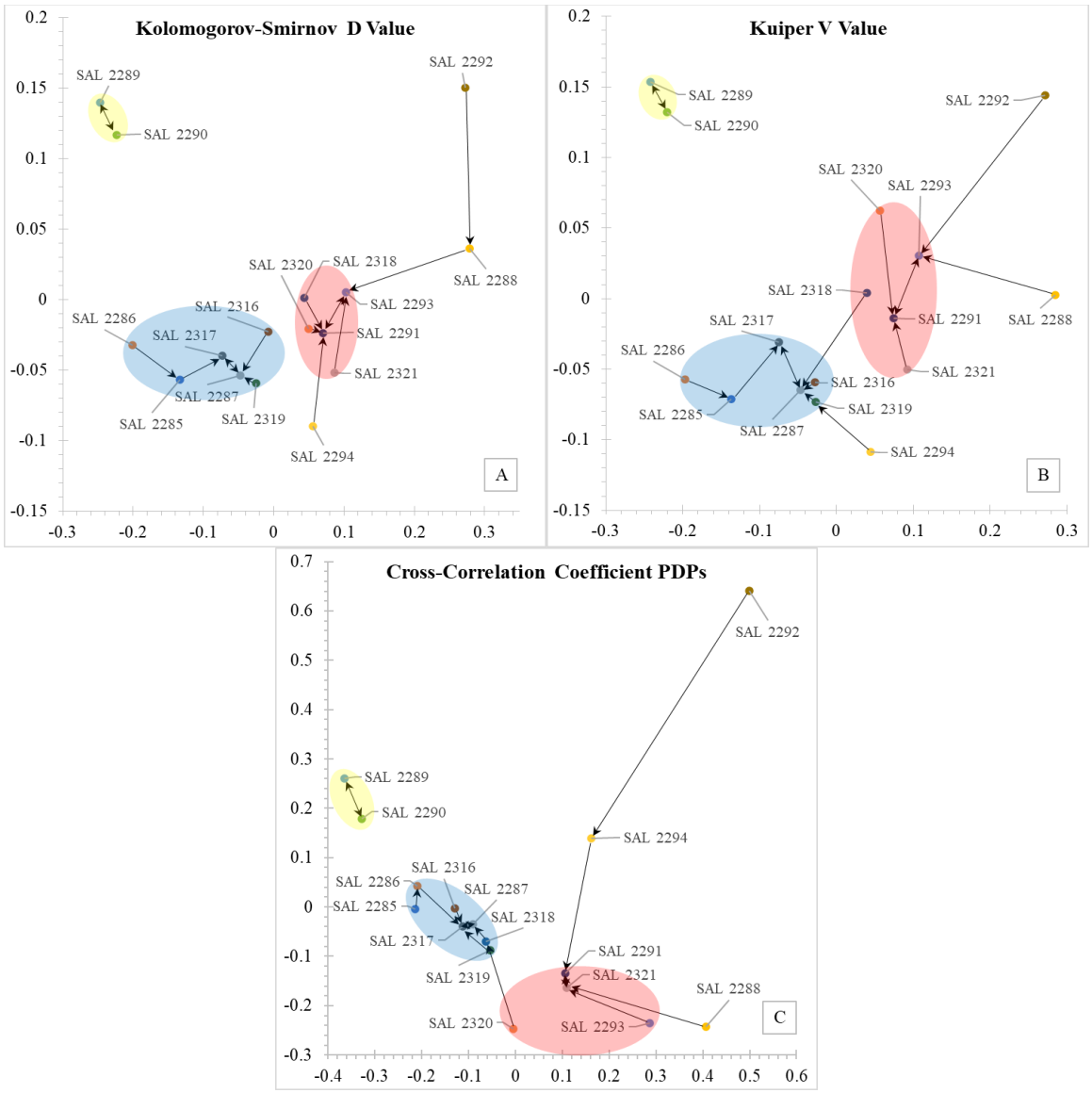

Figure 9. **MDS plots of site U1522 detrital zircon U-Pb dates**

Plots are shown in two dimensions and include only dates less than 1,250 Ma. Plot A uses the D statistic of the two-sample Kolmogorov-Smirnov test to determine if pairs of samples are drawn from the same parent population, plot B uses the two-sample Kuiper test V statistic to make a similar determination, and plot C uses the coefficient of determination, R^2 value, from the cross plot of the samples' probability density plots (Saylor & Sundell, 2016). Black arrows point towards the closest relative of each sample.

All tests indicate that SALs 2292, 2288, and 2294 are outliers. SALs 2289 and 2290 (yellow transparency) have a strong association with one another but not with other samples. The remainder of the samples plot loosely as two groups, one highlighted in blue and the other in the red. The spatial and grouping relationships are relatively similar for all three tests. Note that the scales of the axes for the different comparisons are not uniform and that the axes are dimensionless numbers used only to approximate the original dissimilarity between samples (Saylor & Sundell, 2016).

NEODYMIUM ISOTOPE RESULTS

Neodymium isotopic analysis was performed on twenty-three samples from unique core intervals of site U1522 by J. Marschalek at University College London. Thirteen samples were selected from identical intervals as those analyzed for U-Pb isotopes and an additional ten were chosen from intervals where zircon U-Pb analysis was not performed. This design allowed comparison of U-Pb with neodymium isotopic data at identical depth intervals and provided a means of tracing provenance on intervals of site U1522 that were not analyzed for zircon U-Pb.

Neodymium isotope values (εNd) for all samples occupy a relatively narrow range between more radiogenic ~-5.0 to less radiogenic ~-9.5 values. However, four groups (A-D) of samples are separated by abrupt changes in εNd (Figure 10). The εNd, including their standard deviations, of all samples in each group were averaged to show mean values for sample groups (Figure 10). The lowermost eight samples comprise a group spanning ~165 meters deposited in the late Miocene. The mean εNd of this group (A) is -7.06±0.30 with the most and least radiogenic samples having values of -6.57±0.31 and -7.35±0.31 respectively (Appendix B). Above this, is a group of five samples (B) deposited in the latest Miocene spanning ~105 meters. Its mean εNd is -8.74±0.29 with low and high values of -9.48±0.31 and -7.58±0.31. The next group upcore (C) consists of five samples spanning ~114 meters and deposited in the Pliocene. It has a mean εNd of -5.30±0.26 with low and high values of -6.05±0.25 and -5.03±0.25. From ~227 meters below the seafloor to the core top (latest Pliocene to late Pleistocene deposition), a group of five samples (D) has a mean εNd of -7.96±0.28 with low and high values measured at -8.71±0.29 and -7.53±0.29 respectively.

The lowermost sample group (A) (Figure 10) has the least variation in εNd. As a group, it's mean εNd is also nearest to the combined mean εNd for all site U1522 samples. Sample group B has the widest range of εNd; however, they are also generally the least radiogenic values. These include the lowest εNd measured for any sample. An increasing εNd trend is evident upcore through this group. An abrupt change occurs in a span of less than two meters (~397 meters below the seafloor) and marks a shift to the highest εNd which appear in sample group C. Those values trend slightly towards less radiogenic upcore. The range of εNd in the uppermost group (D) are less radiogenic than all other values from site U1522 with the exception of three or four samples in group B.

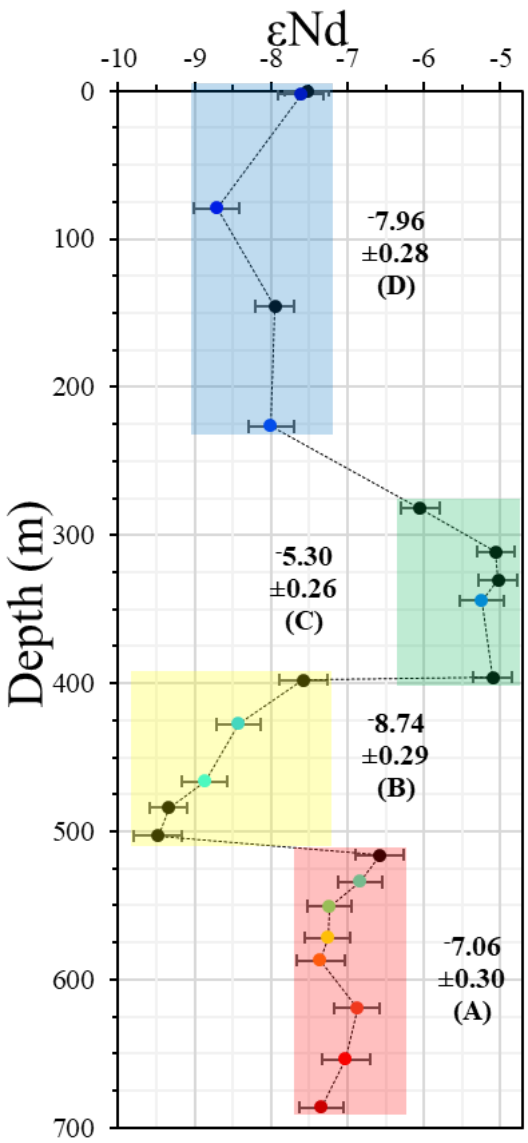

Figure 10. **Neodymium isotope values (εNd) of 23 samples from site U1522**

Samples that were analyzed for U-Pb as well as εNd are shown as colored dots and correspond to those on Figures 8, 9, and 12. The black dots are samples run only for εNd. Values are reported in Appendix 2. Transparent colored rectangles highlight sample groups. Groupings are defined by abrupt variations in εNd between neighboring samples. The mean and mean standard deviation for each group of values is shown in bold beside each transparency.

CLAST DISTRIBUTION RESULTS

Petrographic analysis was done for the lowest ~487 meters of site U1522 on cores 22 through 76 by M. Perotti and L. Zurli at the University of Siena, Italy to understand the lithologic context of the rock types eroded from the Antarctic continental interior into the central Ross Sea since the late Miocene. The relative distribution of five clast types recorded is shown in Figure 11. Metamorphic clasts are the most abundant type through the length of site U1522. Granitoid clasts are the second most abundant. Increasingly smaller components of the clast distribution include basaltic, porphyry, and dolerite clasts. The total number of clasts recovered and the relative distribution of each clast type changes through different depths/core intervals and not all clast types are present at all depths. Gaps exist in the clast distribution log through cores 74, 61, 44-39, 25, and 21-1 where sediment recovery was poor. The clast distribution is assessed in four intervals spanning the late Miocene through the latest Pliocene (groups A-D) below (Figure 11).

From ~696-551 meters below the sea floor (mbsf) (group A), deposited in the late Miocene, the proportion of metamorphic to granitoid clasts ranges between approximately 2:1 to 5:4. Basaltic and porphyry clasts each comprise approximately five to ten percent of the distribution, their highest abundance throughout core U1522. Dolerite is not present (excluding a single clast in core 76). Between ~549-386 mbsf (group B), deposited in the latest Miocene, the proportion of metamorphic to granitoid clasts increases from 2:1 to approximately 4:1. The proportions of both basaltic and porphyry clasts greatly recede midway through this interval near core 55. Dolerite clasts compose ~0.5-2% of the distribution and appear where basaltic and porphyry clasts decline. In the interval ~350-242 mbsf (group C), deposited through the middle Pliocene,

the proportion of granitoid to metamorphic clasts rebounds to ratios approximately intermediate of intervals A and B. The proportions of basaltic and porphyry clasts return to levels similar to those seen in the middle of interval B. Dolerite clasts are absent in the lower ~70 meters of C but reappear in its upper ~30 meters. In the uppermost interval, ~228-209 mbsf (group D), deposited in the latest Pliocene, the proportion of metamorphic to granitoid clasts is ~2:1. The proportions of porphyry, basalt, and dolerite clasts are similar to those in interval C between ~272-253 mbsf.

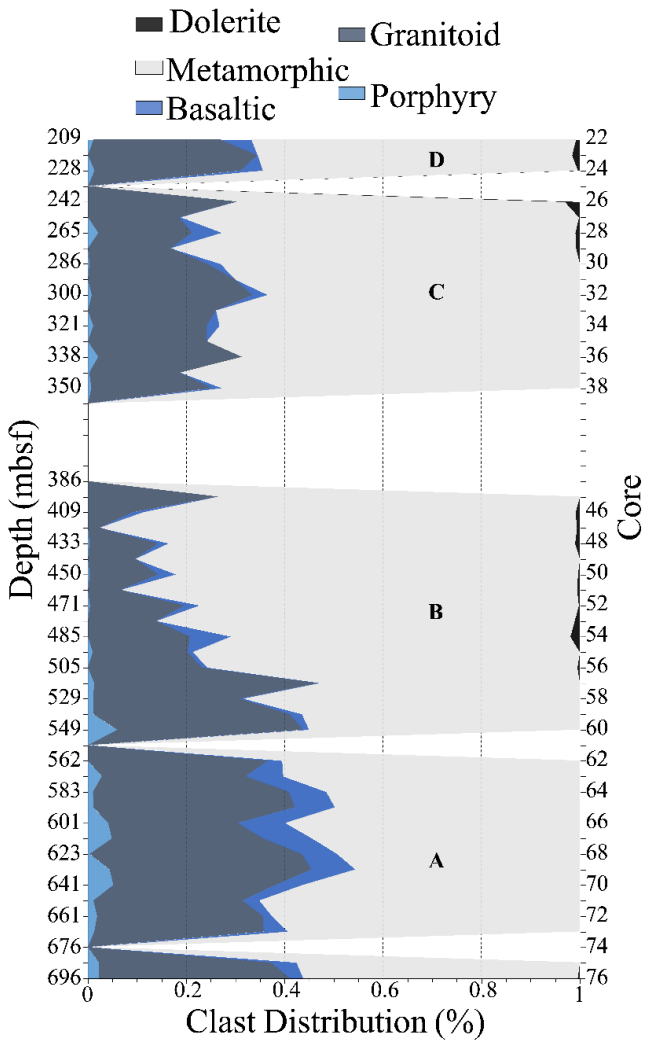

Figure 11. **Clast distribution of the lowest ~487 meters of site U1522**

The distribution is shown as a relative percentage. Sub-intervals described in the results are labeled A, B, C, and D. The distribution of selected clasts are normalized to a fraction of 100% and are shown with a key on the upper x-axis. Gaps in the clast distribution log are due to the poor recovery through those depth intervals. The uppermost ~200 meters of the site were not logged. Basalt and porphyry clasts are more abundant in the lower cores and decrease in relative abundance towards the surface where dolerite clasts begin to appear. Note that where dolerite is present, the total number of clasts observed range between 1 and 7.

DISCUSSION

Datasets reported in this study can individually and collectively indicate provenance changes between East Antarctic versus West Antarctic derived tills and thereby WAIS dominated glacial advances onto the central Ross Sea continental shelf (i.e. across IODP Site U1522) since the late Miocene. The new data are used to assess whether the WAIS converged with ice flowing through the Transantarctic Mountain outlets from East Antarctica during late Miocene glacial maxima as it did during the last glacial maximum (Licht et al., 2014) (Figure 2). Each analytical technique used in this study provides its own insights as to glacial till provenance and therefore to the dynamics of the Antarctic Ice Sheets since the late Miocene, but each has limitations as well. Those limitations have most to do with the ambiguity of provenance interpretations where unique identifiers are not present. Meaning, multiple interpretations of any one data set are possible. Furthermore, even when unique identifiers of provenance are present, they do not rule out the possibility of some mixture of both East and West Antarctic derived sediment. Therefore, it is the amalgamation of evidence garnered from all three of these analyses (zircon U-Pb, εNd, and clast distribution) that provides the clearest and best data backed interpretation of provenance.

Framework for determining U1522 till provenance

Zircon U-Pb isotopic dates are commonly used as a provenance indicators and numerous East Antarctic and West Antarctic source formations that outcrop in the Ross Sea catchment have been extensively dated using this method (e.g., Elliot et al., 2017; Siddoway & Fanning, 2009). Both East and West Antarctic rocks harbor zircon grains from the Mesoproterozoic to the early Jurassic (Figure 5), thus many age populations can

be ambiguous provenance tracers when viewed alone. In contrast, Cretaceous zircon dates have only been found from zircon grains from beneath two northerly West Antarctic Ice Streams, Kamb and Bindschadler (Licht et al., 2014) (Figure 2) and in the Byrd Coast Granite, Fosdick Migmatite-Granite Complex, and other metasedimentary rocks of Marie Byrd Land in West Antarctica (Korhonen et al., 2009; Yakymchuk et al.,2015). Thus, the presence of Cretaceous zircons in sediment of site U1522 indicates West Antarctic provenance.

Neodymium values that are less radiogenic or more negative (i.e., -8.6 or less), are consistent with values derived from a mixture of East Antarctic sources (Marschalek et al., 2021) (Figure 6). Neodymium values that are more radiogenic or more positive (i.e., -7.2 or greater) have better accordance with signals composed of a mixture of West Antarctic sources (Marschalek et al., 2021) (Figure 6). A caveat to this generality is that a mixture of East and West Antarctic source lithologies can produce a neodymium signal that may be indistinguishable from a signal derived primarily from one or the other (Figure 6) (Farmer & Licht, 2016). As neodymium isotopic analysis is measured on the less than 63-micron sediment fraction (silt and clay particles), it may be interpreted as a representative mixture of the diversity of parent assemblages in a catchment, however the results of it may not explicitly agree with the results of other analyses due to fractional sorting biases (i.e. Malusa et al., 2016) or variability in the robustness of sample sizes.

Many rock types are common to formations that outcrop in both East and West Antarctica (in the Ross Sea catchment) and so those lithologies may be poor individual indicators of provenance. For example metasedimentary and metamorphic lithologies are common to the Nimrod Group, Beardmore Group, and Byrd Group of East Antarctica

(Elliot & Fanning, 2008; Elliot et al., 2014; Elliot et al., 2016; Elliot et al., 2017; Paulsen et al., 2017; Goodge et al., 2001; Goodge et al., 2002) as well as the Swanson Formation, Fosdick Migmatite-Granite Complex, and Whitmore Mountains crustal block of West Antarctica (Pankhurst et al., 1998; Yakymchuk et al., 2015; Korhonen et al., 2009; Siddoway & Fanning, 2009; McFadden et al., 2010; Flowerdew et al., 2007). Granitoid lithologies are common to the Granite Harbor Intrusive Complex of East Antarctica, which outcrops extensively through the Transantarctic Mountains, and also West Antarctica's Ford Granodiorite and Fosdick Migmatite-Granite Complex (Figure 4) (Goodge et al., 2012; Pankhurst et al., 1998; Yakymchuk et al., 2015; Korhonen et al., 2009; Siddoway & Fanning, 2009). Basalt is seen in the Kirkpatrick Basalts of the Ferrar Large Igneous Province of East Antarctica (Burgess et al., 2015) but is sparse in West Antarctic outcrops (e.g. Siddoway et al., 2008; Jordan et al., 2020). However, felsic-basaltic shield volcanoes are seen in the far eastern portion of the Marie Byrd Land Igneous Province (Rocci et al., 2006) and widespread basaltic volcanism associated with the mid-Cenozoic West Antarctic Rift System is suggested by aeromagnetic studies (Behrendt et al., 1995; van Wyk de Vries et al., 2017). Porphyries are an unusual texture uncommon in bedrock of East or West Antarctica and thus are not decisively useful as a provenance tracer. Dolerite of the Ferrar Group crops out extensively through the Transantarctic Mountains, however it is not common to outcrops in West Antarctica (Burgess et al., 2015). Therefore, the presence of dolerite in cores/intervals from site U1522 is interpreted to indicate East Antarctic derived sediments.

U1522 till provenance interpretations

Late Miocene (lithologic units IV-IIIB)

The late Miocene interval has relatively uniform εNd values (mean of -7.06±0.30) which are consistent with a mixture of West Antarctic derived sources (Figures 6 & 12). Numerous Cretaceous zircon U-Pb dates throughout this interval indicate sediment input from West Antarctica (Figure 12). This means that the Ross and Grenville age peaks herein are most likely an assemblage eroded from Swanson Formation and western Marie Byrd Land metasedimentary rocks, with possible input from the Whitmore Mountain group. Furthermore, the Ross Orogeny (c. 470-615 Ma) dates through this interval are dominantly at the younger end of the range of Ross ages, which corresponds better with WAIS tills and bedrock sources than with East Antarctic glacier tills and bedrock sources (Figure 5). The numerous Triassic-Jurassic age dates do not have an obvious source in West Antarctica that has been dated, which suggests an unmapped subglacial terrain of this age due to it being coupled with numerous Cretaceous dates. However, the Triassic-Jurassic dates in this interval could also reflect an East Antarctic signal or a signal from the Fosdick Migmatite-Granite Complex (Fosdick Metamorphics) (Figure 5). Two samples in this late Miocene core interval have substantial numbers of anomalous ~34 Ma zircon grains that do not have clear analogues in the East Antarctic or West Antarctic geologic zircon records. The significance of these is discussed below. The lithologic distribution is also consistent with West Antarctic source rocks as dolerite clasts are absent through this interval (with the exception of a single clast in core 76) (Figure 12). The basaltic clasts may be primarily derived from the Marie Byrd Land Igneous Province, the granitoid clasts from the Byrd Coast Granite or Fosdick

Migmatite-Granite Complex, and the metamorphic clasts from some mixture of the Swanson Formation, Fosdick Migmatite-Granite Complex and Whitmore Mountain block.

Latest Miocene (lithologic units IIIB-IIIA)

The latest Miocene interval is characterized by typically less radiogenic εNd with a mean of -8.74±0.29 that is consistent with erosion of primarily East Antarctic bedrock also seen in last glacial maximum tills derived from the Transantarctic Mountains (Farmer et al., 2006; Marschalek et al., 2021) (Figures 6 & 12). Neodymium values increase through this interval from -9.48±0.31 to -7.58±0.31 suggesting a steady decline in East Antarctic derived sediment (Figure 12). Zircon U-Pb dates from this interval are dominated by large Ross Orogeny peaks with abundant older Ross dates (~580-615 Ma) and are accompanied by very few Triassic-Jurassic or Cretaceous dates (Figure 12). The sparse number of Cretaceous-age zircons suggest minor input from West Antarctic bedrock/tills or incorporation of them as ice advanced over older tills. The assemblage of Grenville and Ross aged U-Pb peaks fits nicely with an assemblage of zircon U-Pb dates derived from the Beacon Supergroup, Granite Harbor Intrusives, and the Byrd and Beardmore Groups (Figures 5 & 12). Dolerite is present throughout this interval indicating East Antarctic input from the Ferrar Large Igneous Province. Basalt and granitoid clasts decrease in proportion through this interval while metamorphic clasts increase. This suggests the Kirkpatrick Basalts of the Transantarctic Mountains or the McMurdo Volcanics as the basaltic source (Burgess et al., 2015; Goodge, 2019). Given that dolerite is present, the coeval Kirkpatrick Basalts are a more likely basalt source. The proportion of metamorphic to granitoid clasts are consistent with a mixed input of the

abundant metasedimentary, metamorphic, and granitoid lithologies that comprise much of the Transantarctic Mountain formations including the Beacon Supergroup, Nimrod Group, Beardmore Group, Byrd Group, and Granite Harbor Intrusive series (Elliot & Fanning, 2008; Elliot et al., 2014; Elliot et al., 2016; Elliot et al., 2017; Paulsen et al., 2017; Goodge et al., 2001; Goodge et al., 2002; Goodge et al., 2012; Goodge, 2019) (Figures 4 & 12).

Early to mid-Pliocene (lithologic unit II)

Neodymium isotopes shift very sharply (over less than 1.65 meters) at the contact of the latest Miocene-early Pliocene interval from a less radiogenic value of -7.58±0.31 to a more radiogenic value of -5.10±0.25. The early to mid-Pliocene interval is characterized by the most radiogenic εNd with a mean of -5.30±0.26, which is consistent with a West Antarctic provenance (Figures 6 & 12). The uppermost mid-Pliocene sample has a εNd of -6.05±0.25, which is less radiogenic than all other Pliocene values, suggesting an increase in East Antarctic input toward the latest Pliocene. A single sample represents the zircon U-Pb data available for this interval (Figure 12). It is dominated by Cretaceous and Triassic-Jurassic peaks with minor Ross and Grenville aged peaks. However, Ross-age zircons are dominantly younger dates, similar to the late Miocene core interval. The large Cretaceous peaks firmly indicate sediments derived from West Antarctica and being coupled to numerous early-mid Mesozoic dates, support the suggestion of an unexposed Triassic-Jurassic terrain beneath the WAIS. No dolerite is present from the latest Miocene-early Pliocene contact through the mid-Pliocene, consistent with minimal East Antarctic input through this interval. Basaltic, granitoid, and metamorphic clasts are likely primarily derived from West Antarctic bedrock sources

including the Marie Byrd Land Igneous Province, Byrd Coast Granite, Fosdick Migmatite-Granite Complex, and Swanson Formation.

Latest Pliocene-Pleistocene (lithologic units II & I)

The latest Pliocene-Pleistocene interval is characterized by less radiogenic εNd with a mean of -7.96±0.28 characteristic of a mixture of East Antarctic sources (Figures 6 & 12), though sampling density is lower than in other time intervals. Dolerite reemerges in the clast distribution data near the assumed lower contact of this provenance interval (Figures 11 & 12), which also suggests an East Antarctic provenance. Zircon U-Pb dates are dominated by Ross age peaks with increasingly smaller numbers of Triassic-Jurassic and Grenvillian zircons (Figure 12). Few Cretaceous zircon grains are present, suggesting diminished West Antarctic sediment input. Triassic-Jurassic dates are likely derived from the Beacon Supergroup due to the tandem scarcity of Cretaceous zircon grains.

Ice sheet history from U1522 provenance

Glaciation has played a considerable role in sculpting Antarctica's topography which itself exerts a fundamental influence on the dynamics of the Antarctic Ice Sheets (Paxman et al., 2019). Modern ice divides and flow directions (i.e. Rignot et al., 2019) (Figure 1-C) are the best approximation of the Ross Sea catchment since the inception of the Antarctic Ice Sheets in the early Oligocene (e.g. Zachos et al., 2001). Neodymium values from early Miocene intervals of IODP site U1521 suggest excursions of a grounded WAIS onto the central Ross Sea continental shelf as early as ~17.8 Ma, millions of years prior to the Miocene Climatic Transition (Marschalek et al., 2021).

Glacigenic diamictites deposited on the central Ross Sea continental shelf at site U1522 record the ice sheet history of Antarctica since the late Miocene ~11 Ma and shifts

in provenance associated with Ross Sea Unconformities 2 and 3. Late Miocene tills have abundant Cretaceous zircons, more positive neodymium values, and lack dolerite clasts which suggests ice sheet advances were dominated by West Antarctic ice in that time. An abrupt provenance shift in the latest Miocene suggests ice sheet advances were dominated by East Antarctic ice as evidenced by the few numbers of Cretaceous zircons, more negative neodymium values, and abundant dolerite clasts in those tills. Ross Sea Unconformity 3, at the latest Miocene-Pliocene, is likely an erosional record of the shift from East Antarctic to West Antarctic dominated ice advances, which is most clearly reflected by the neodymium isotope data (Figure 12). Early to mid-Pliocene tills suggest West Antarctic dominated ice advances evidenced in numerous Cretaceous zircons, more positive neodymium values, and lack of dolerite clasts. Ross Sea Unconformity 2, in the mid-Pliocene, is likely an erosional record of the shift from West Antarctic to East Antarctic dominated ice advances which is most clearly reflected by the appearance of dolerite in the clast data. It should be noted that the total number of dolerite clasts counted in any given core were in the single digits (ranging between 1 and 7). This means that provenance assumptions based primarily on the clast distribution data could be more sensitive to error. Latest Pliocene to Pleistocene advances were increasingly dominated by East Antarctic ice as suggested by fewer Cretaceous zircons, more negative neodymium values and the presence of dolerite in those tills. Provenance shifts associated with Ross Sea Unconformities 3 and 2 cored at site U1522 are also reflected in changes in the zircon U-Pb dates from sampled core intervals (Figure 12).

The stratigraphic record of advance and retreat cycles of late Miocene to late Pleistocene sediments deposited at AND-1B is thought to be intimately tied to the overall

state of the West Antarctic Ice Sheet (McKay et al., 2009). Although the AND-1B record lacks the detail of multiple provenance proxies measured on site U1522 tills, late Miocene-Pliocene clast distributions from AND-1B suggest that provenance shifts between different sectors of the Transantarctic Mountain outlets might be tied to regional changes in the ice contributions of the East versus the West Antarctic ice sheet (Talarico et al., 2009). Furthermore, clast analysis on glacially derived diamicts of late Pliocene to Pleistocene depositional age show a strong Transantarctic Mountain provenance (Talarico et al., 2009) with an increase in Beacon Supergroup and dolerite clasts in the late Pleistocene (Talarico et al., 2010). Additionally, petrologic analysis of diamictite thin sections from AND-1B show less Transantarctic Mountain influence in the Pliocene whereas Pleistocene diamictites contain distinct Transantarctic Mountain provenance (Pompilio et al., 2007). Provenance changes seen in site U1522 tills support these interpretations with three new datasets. Specifically, data from site U1522 indicate that West Antarctic dominated ice advances in the late Miocene rapidly gave way to East Antarctic dominated advances in the latest Miocene. An abrupt provenance shift coincident with RSU 3 at the start of the Pliocene indicates a change to West Antarctic dominated advances through the mid Pliocene. In the middle to late Pliocene, and most likely coincident with RSU 2, advances switched back to East Antarctic dominated (Figure 12).

Implications for subglacial geology

Detrital zircons from three late Miocene samples from site U1522 yielded previously unseen dates ~34 Ma (Figure 12). Core 59 contained only a single grain of this age but cores 63 and 75 each had numbers in the double digits (Appendix A). Given that

these ~34 Ma dates are intermingled among an interval with West Antarctic provenance (Figure 12), it is more likely these zircons originated from a West Antarctic source. However, these dates are not present in all the samples in this interval, nor are they present in the Pliocene sample (SAL 2288) with West Antarctic provenance (Figure 12). Aeromagnetic data suggests the presence of subglacial volcanic centers beneath the WAIS associated with late/ongoing activity of the West Antarctic Rift System which could be the source rocks for these zircons (Behrendt et al., 2005; van Wyk de Vries et al., 2017). This would require that ice entrain sediments from a volcanic edifice of this age and deposit them at site U1522. This may occur intermittently as the ice flow pathway (e.g. Licht et al., 2014) (Figure 2) changes over time. If ice flow pathway changes, it may not entrain the ~34 Ma source, or it may deposit those sediments elsewhere (or both). Ages proposed for the emplacement of the Dorrel Rock Igneous Complex in far eastern Marie Byrd Land (Rocci et al., 2006) fit nicely with the ~34 Ma zircon dates from site U1522. This solution would necessitate that the Dorrel Rock igneous activity extended inland into West Antarctica's Ross Sea catchment and is currently unexposed due to ice cover.

Triassic-Jurassic zircons are ubiquitous in site U1522 cores but are in greater abundance in intervals that also contain more Cretaceous zircons (i.e. the late Miocene and early Pliocene) (Figure 12). Due to this association, most Triassic-Jurassic zircons in these intervals are inferred to be of West Antarctic origin, however there are few exposures in that region that have yielded such dates (e.g. the Fosdick Migmatite Granite Complex) (Siddoway & Fanning, 2009) (Figure 5). Moreover, Triassic-Jurassic zircons dominate some formations of the Beacon Supergroup of East Antarctica (Elliot &

Fanning, 2008; Elliot et al., 2016; Elliot et al., 2017; Paulsen et al., 2017), which could make it seem a more appropriate source (Figure 5). However, were these dates derived primarily from East Antarctic sources, their fingerprint would also be greater in SAL 2289 and SAL 2290 and reflected in the clast distribution and neodymium data through that interval (Figure 12). This suggests the presence or former presence of an extensive Triassic-Jurassic terrain beneath the WAIS. Potential inputs could be further evaluated using a mixing model (e.g. DZmix) to quantitatively propose bedrock and till sources for Triassic-Jurassic zircon dates.

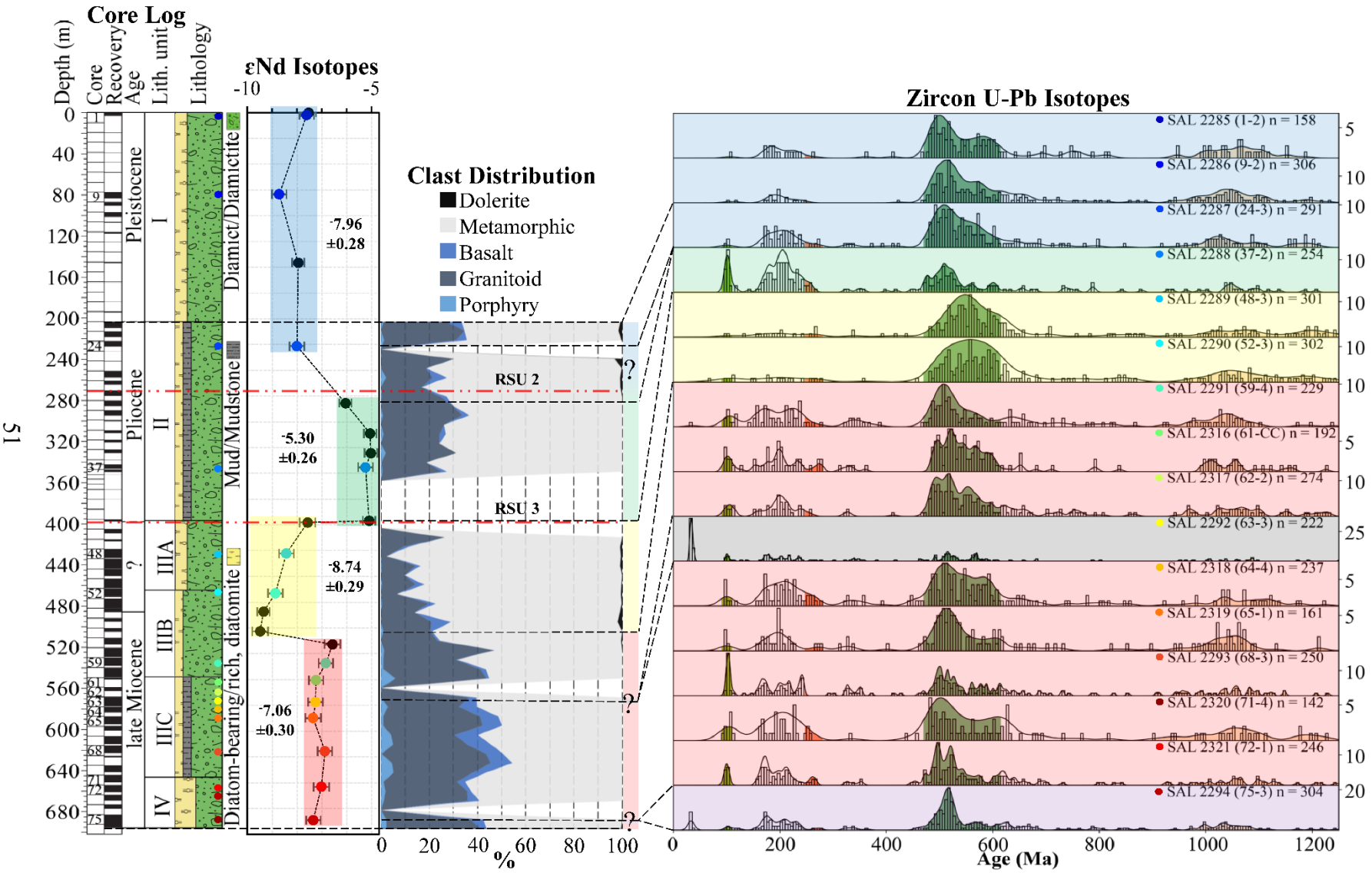
Core Log
Depth (m)
Core Recovery
Age
Lith. unit
Lithology
εNd Isotopes
-10
-5
Clast Distribution
Dolerite
Metamorphic
Basalt
Granitoid
Porphyry
Zircon U-Pb Isotopes
Pleistocene
Pliocene
late Miocene
?
I
II
IIIA
IIIB
IIIC
IV
Diamict/Diamictite
Mud/Mudstone
Diatom-bearing/rich, diatomite
-7.96 ±0.28
-5.30 ±0.26
-8.74 ±0.29
-7.06 ±0.30
RSU 2
RSU 3
SAL 2285 (1-2) n = 158
SAL 2286 (9-2) n = 306
SAL 2287 (24-3) n = 291
SAL 2288 (37-2) n = 254
SAL 2289 (48-3) n = 301
SAL 2290 (52-3) n = 302
SAL 2291 (59-4) n = 229
SAL 2316 (61-CC) n = 192
SAL 2317 (62-2) n = 274
SAL 2292 (63-3) n = 222
SAL 2318 (64-4) n = 237
SAL 2319 (65-1) n = 161
SAL 2293 (68-3) n = 250
SAL 2320 (71-4) n = 142
SAL 2321 (72-1) n = 246
SAL 2294 (75-3) n = 304
%
Age (Ma)
51

Figure 12. **Compilation of site U1522 data**

From left to right: core log, neodymium log, clast distribution log, and zircon U-Pb isotopes of Site U1522 samples. On the core log, CSF-A is core depth below seafloor in meters. Percent recovery for each core is indicated by the blacked-out area beside core rectangles. Age units are assigned based on microfossil assemblages however reworking of intervals 1-CC to 22-3 and 46-CC to 54-CC makes age assignment through these intervals difficult (McKay et al., 2019[a]). However, reworking may suggest ice overriding. Lithologic units were defined by visual core description, microscopic examination of smear slides, and color spectral observations (McKay et al., 2019[a]). The lithology column shows the relative proportions of the dominant lithologies through the units. The depth scale on the core log is aligned to the rest of the figure with dotted black lines. The neodymium log shows the individual radiogenic values of twenty-three samples where more negative values indicate older sediments. The average neodymium values of several groups of samples appears in bold near each grouping and the absolute value of each is shown on the x-axis. The clast distribution log denotes the relative proportion (x-axis) of five different clast lithologies by core/depth for site U1522 for intervals from cores 76 to 22. Red dotted lines through the core log, neodymium isotope chart, and clast distribution mark the approximate location of Ross Sea Unconformities (RSU) 2 and 3. The zircon U-Pb isotopes plot shows a five-million-year bin histogram with an adaptive-fixed kernel density estimate of detrital zircon analyses from each sample. The sample name, core-section, and number of analyses appear in the upper right corner of each histogram. Peak height in number of grains analyzed (n) appears on the y-axis and age in Ma is on the x-axis. Colored areas under the kernel density estimate mark several zircon producing events which include the

Grenville, Ross and Gondwanide Orogenies and Cretaceous volcanism associated with the West Antarctic Rift System. Colored dots on the core log, neodymium log, and zircon U-Pb isotopes are correspond between the different plots. Colored rectangular transparencies on the neodymium, clast distribution, and zircon plots overlay sample groupings. Transparencies that appear only on the zircon plot (back and purple) indicate samples with visually different zircon populations but similar neodymium and clast distribution values. Question marks on the clast distribution denote intervals that are unsampled or known to be different than other samples in the surrounding group based on their zircon signatures.

CONCLUSIONS

Multi-suite provenance analysis is of particular value to interpreting the ice sheet history of Antarctica because more confidence is offered with combined datasets. The coupled zircon U-Pb, neodymium isotope, and clast distribution data from site U1522 indicates four primary oscillations of East versus West Antarctic dominated ice in the central Ross Sea during the late Miocene, latest Miocene, early to mid-Pliocene, and latest Pliocene through late Pleistocene, respectively. Provenance proxies indicate that the WAIS likely advanced to the Ross Sea continental shelf edge at times during the early to mid-Pliocene which therefore will help constrain Antarctic ice sheet contributions to sea level lowstands through that time (e.g. McKay et al., 2019[a]; Naish et al., 2009).

Zircon samples from site U1522 indicate a complementary association between Triassic-Jurassic and Cretaceous dates, which suggests unidentified bedrock terrains in West Antarctica of early-mid Mesozoic age. This relationship is most obvious in early to mid-Pliocene sediments when the WAIS dominated the provenance signature of U1522 tills. If this is so, zircon U-Pb analysis of additional Pliocene intervals from U1522 should show similar zircon age distributions. Previously unreported Eocene-Oligocene zircons are also attributed to tills of late Miocene deposition with West Antarctic provenance, perhaps suggesting the Dorrel Rock Igneous Province extends southwestward into West Antarctica or that subglacial volcanic edifices of that age existed/exist below the WAIS.

The higher resolution sampling intervals for neodymium and clast distribution data provide the clearest signal of the provenance changes associated with Ross Sea Unconformities 3 (end Miocene) and 2 (mid-Pliocene) and indicate abrupt shifts between East and West Antarctic

ice excursions. The provenance shift in late Miocene lithologic unit IIIB is comparably abrupt to Ross Sea Unconformities 3 and 2 (Figure 12). An additional neodymium sample that brackets the late Pliocene interval of Ross Sea Unconformity 2 would help illustrate how abrupt the shift from West to East Antarctic dominated ice excursions were at that time. A second zircon sample from the earliest Pliocene could support the suggestion of an abrupt WAIS excursion associated with Ross Sea Unconformity 3 seen in the neodymium data, where clast data is unavailable.

APPENDICES

Appendix A

SUPPLEMETARY TABLE 1. ZIRCON U-Pb DATA

Appendix B

SUPPLEMENTARY TABLE 2. εNd DATA

SAL #	Core	Section	Top Offset (cm)	Bottom Offset (cm)	Midpoint Depth (m)	εNd	2SD
NA	1	1	2	5	0.035	-7.53	0.29
2285	1	2	60	90	2.27	-7.61	0.29
2286	9	2	30	70	79.3	-8.71	0.29
NA	16	1	44	46	145.65	-7.95	0.25
2287	24	3	100	140	226.6	-8.00	0.29
NA	30	2	38	41	281.895	-6.05	0.25
NA	33	2	110	113	311.285	-5.06	0.25
NA	35	2	83	86	330.355	-5.03	0.25
2288	37	2	10	60	344.25	-5.24	0.29
NA	45	1	56	59	396.075	-5.10	0.25
NA	45	2	69	72	397.725	-7.58	0.31
2289	48	3	20	60	427.82	-8.42	0.29
2290	52	3	40	80	466.33	-8.87	0.29
NA	54	2	64	67	484.215	-9.34	0.25
NA	56	2	36	39	503.135	-9.48	0.31
NA	57	4	82	85	515.875	-6.57	0.31
2291	59	4	20	60	534.19	-6.83	0.29
2316	61	CC	5	27	550.68	-7.23	0.29
2317	NA	NA	NA	NA	NA	NA	NA
2292	63	3	37	77	571.75	-7.26	0.29
2318	NA	NA	NA	NA	NA	NA	NA
2319	65	1	0	11	587.355	-7.35	0.31
2293	68	3	85	125	619.42	-6.88	0.29
2320	NA	NA	NA	NA	NA	NA	NA
2321	72	1	14	25	653.995	-7.02	0.31
2294	75	3	65	105	686.31	-7.34	0.29

REFERENCES

Anderson, J.B., Conway, H., Bart, P.J., et al. (2014). Ross Sea paleo-ice sheet drainage and deglacial history during and since the LGM. Quaternary Science Reviews 100: 31-54.

Behrendt, J.C., Blankenship, D.D., Damaske, D., et al. (1995). Glacial removal of late Cenozoic subglacially emplaced volcanic edifices by the West Antarctic ice sheet. Geology 23(12): 1111-1114.

Black, L.P., Kamo, S.L., Allen, C.M., et al. (2004). Improved 206Pb/238U microprobe geochronology by the monitoring of a trace-element-related matrix effect; SHRIMP, ID-TIMS, ELA-ICP-MS and oxygen isotope documentation for a series of zircon standards. Chemical Geology 205(1-2): 115-140.

Burgess, S.D., Bowring, S.A., Fleming, T.H., et al. (2015). High-precision geochronology links the Ferrar large igneous province with early-Jurassic ocean anoxia and biotic crisis. Earth and Planetary Science Letters 415: 90-99.

Dalziel, I. W. D. (2013). Antarctica and supercontinental evolution: clues and puzzles. Earth and Environmental Science Transactions of the Royal Society of Edinburgh 104(1): 3-16.

Elliot, D.H. and Fanning, C.M. (2008). Detrital zircons from upper Permian and lower Triassic Victoria Group sandstones, Shackleton Glacier region, Antarctica: Evidence for multiple sources along the Gondwana plate margin. Gondwana Research 13(2): 259-274.

Elliot, D.H. and Fleming, T.H. (2008). Physical volcanology and geological relationships of the Jurassic Ferrar Large Igneous Province, Antarctica. Journal of Volcanology and Geothermal Research 172(1-2): 20-37.

Elliot, D.H. (2013). The geological and tectonic evolution of the Transantarctic Mountains: a review. Geological Society, London, Special Publications 381(1): 7-35.

Elliot, D.H., Fanning, C.M., and Hulett, S.R.W. (2014). Age provinces in the Antarctic craton: Evidence from detrital zircons in Permian strata from the Beardmore Glacier region, Antarctica. Gondwana Research 28(1): 152-164.

Elliot, D.H., Larsen, D., Fanning, C.M., et al. (2016). The Lower Jurassic Hanson Formation of the Transantarctic Mountains: implications for the Antarctic sector of the Gondwana plate margin. Geological Magazine 154(4): 777-803.

Elliot, D.H., Fanning, C.M., Isbell, J.L., et al. (2017). The Permo-Triassic Gondwana sequence, central Transantarctic Mountains, Antarctica: Zircon geochronology, provenance, and basin evolution. Geosphere 13(1): 155-178.

Farmer, G.L., Licht, K., Swope, R.J., et al. (2006). Isotopic constraints on the provenance of fine-grained sediment in LGM tills from the Ross Embayment, Antarctica. Earth and Planetary Science Letters 249(1-2): 90-107.

Farmer, G.L. and Licht, K.J. (2016). Generation and fate of glacial sediments in the central Transantarctic Mountains based on radiogenic isotopes and implications for reconstructing past ice dynamics. Quaternary Science Reviews 150: 98-109.

Fielding, C.R., Browne, G.H., Florindo, F., et al. (2011). Sequence stratigraphy of the ANDRILL AND-2A drillcore, Antarctica: A long-term, ice-proximal record of Early to Mid-Miocene climate, sea-level and glacial dynamism. Palaeogeography, Palaeoclimatology, Palaeoecology 305(1-4): 337-351.

Flowerdew, M.J., Millar, I.L., Curtis, M.L., et al. (2007). Combined U-Pb geochronology and Hf isotope geochemistry of detrital zircons from early Paleozoic sedimentary rocks, Ellsworth-Whitmore Mountains block, Antarctica. Geological Society of America Bulletin 119(3-4): 275-288.

Gehrels, G., Valencia, V., and Pullen, A. (2006). Detrital Zircon Geochronology by Laser-Ablation Multicollector ICPMS at the Arizona LaserChron Center. The Paleontological Society Papers **12**: 67-76.

Gehrels, G.E., Valencia, V., and Ruiz, J. (2008). Enhanced precision, accuracy, efficiency, and spatial resolution of U-Pb ages by laser ablation-multicollector-inductively coupled plasma-mass spectrometry. Geochemistry, Geophysics, Geosystems **9**(3): 1-13.

Goodge, J.W., Fanning, C.M., and Bennett, V.C. (2001). U-Pb evidence of 1.7 Ga crustal tectonism during the Nimrod Orogeny in the Transantarctic Mountains, Antarctica: implications for Proterozoic plate reconstructions. Precambrian Research 112: 261-288.

Goodge, J.W., Myrow, P., Williams, I.S., et al. (2002). Age and Provenance of the Beardmore Group, Antarctica: Constraints on Rodinia Supercontinent Breakup. The Journal of Geology 110: 393-406.

Goodge, J.W., Fanning, C.M., Norman, M.D., et al. (2012). Temporal, Isotopic and Spatial Relations of Early Paleozoic Gondwana-Margin Arc Magmatism, Central Transantarctic Mountains, Antarctica. Journal of Petrology 53(10): 2027-2065.

Harley, S.L., Fitzsimons, I.C.W., and Zhao, Y. (2013). Antarctica and supercontinent evolution: historical perspectives, recent advances and unresolved issues. Geological Society, London, Special Publications 383(1): 1-34.

Howat, I.M., Porter, C., Smith, B.E., et al. (2019). The Reference Elevation Model of Antarctica. The Cryosphere 13(2): 665-674.

Korhonen, F.J., Saito, S., Brown, M., et al. (2009). Multiple Generations of Granite in the Fosdick Mountains, Marie Byrd Land, West Antarctica: Implications for Polyphase Intracrustal Differentiation in a Continental Margin Setting. Journal of Petrology 51(3): 627-670.

LeMasurier, W.E. (1990). Late Cenozoic Volcanism on the Antarctic Plate: An Overview, American Geophysical Union.

Malusà, M.G., Resentini, A., and Garzanti, E. (2016). Hydraulic sorting and mineral fertility bias in detrital geochronology. Gondwana Research 31: 1-19.

Mattinson, J.M. (2010). Analysis of the relative decay constants of 235U and 238U by multi-step CA-TIMS measurements of closed-system natural zircon samples. Chemical Geology 275(3-4): 186-198.

McFadden, R.R., Siddoway, C.S., Teyssier, C., et al. (2010). Cretaceous oblique extensional deformation and magma accumulation in the Fosdick Mountains migmatite-cored gneiss dome, West Antarctica. Tectonics 29(4): n/a-n/a.

McKay, R.M., De Santis, L., and Kulhanek, D.K. (2017). Expedition 374 Scientific Prospectus: Ross Sea West Antarctic Ice Sheet History. International Ocean Discovery Program. https://doi.org/10.14379/iodp.sp.374.2017

McKay, R.M., De Santis, L., Kulhanek, D.K., and the Expedition 374 Scientists. (2018). Expedition 374 Preliminary Report: Ross Sea West Antarctic Ice Sheet History. International Ocean Discovery Program, 374. https://doi.org/10.14379/iodp.pr.374.2018

McKay, R.M., DeSantis, L., Kulhanek, D.K., and the Expedition 374 Scientists. (2019)[a]. Ross Sea West Antarctic Ice Sheet History, Leg 374 Site U1522 Report. Proceedings of the International Ocean Discovery Program, 374. https://doi.org/10.14379/iodp.374.104.2019

McKay, R.M., DeSantis, L., Kulhanek, D.K., and the Expedition 374 Scientists. (2019)[b]. Ross Sea West Antarctic Ice Sheet History, Leg 374 Site U1521 Report. Proceedings of the International Ocean Discovery Program, 374. https://doi.org/10.14379/iodp.374.104.2019

Naish, T.R., Powell, R.D., Barrett, P.J., et al. (2005). ANDRILL McMurdo Ice Shelf Project Scientific Prospectus. ANDRILL Project Information. 7. http://digitalcommons.unl.edu/andrillinfo/7

Naish, T., Powell, R., Levy, R., et al. (2009). Obliquity-paced Pliocene West Antarctic ice sheet oscillations. Nature 458(7236): 322-328.

Nordsvan, A.R., Kirscher, U., Kirkland, C.L., et al. (2020). Resampling (detrital) zircon age distributions for accurate multidimensional scaling solutions. Earth-Science Reviews 204.

Paces, J.B. and Miller, J.D. (1993). Precise U-Pb ages of Duluth Complex and related mafic intrusions, northeastern Minnesota: Geochronological insights to physical, petrogenetic, paleomagnetic, and tectonomagmatic processes associated with the 1.1 Ga Midcontinent Rift System. Journal of Geophysical Research: Solid Earth 98(B8): 13997-14013.

Pankhurst, R.J., Weaver, S.D., Bradshaw, J.D., et al. (1998). Geochronology and geochemistry of pre-Jurassic superterranes in Marie Byrd Land, Antarctica. Journal of Geophysical Research 103: 2529-2547.

Paulsen, T., Deering, C., Sliwinski, J., et al. (2017). Detrital zircon ages and trace element compositions of Permian–Triassic foreland basin strata of the Gondwanide orogen, Antarctica. Geosphere 13(6): 2085-2093.

Perotti, M., Andreucci, B., Talarico, F., et al. (2017). Multianalytical provenance analysis of Eastern Ross Sea LGM till sediments (Antarctica): Petrography, geochronology, and thermochronology detrital data. Geochemistry, Geophysics, Geosystems 18(6): 2275-2304.

Pompilio, M., Dunbar, N., Gebhardt, A.C., et al. (2007). Petrology and Geochemistry of the AND-1B Core, ANDRILL McMurdo Ice Shelf Project, Antarctica. Terra Antartica 14: 255-288.

Pullen, A., Ibáñez-Mejía, M., Gehrels, G.E., et al. (2014). What happens when n= 1000? Creating large-n geochronological datasets with LA-ICP-MS for geologic investigations. J. Anal. At. Spectrom. 29(6): 971-980.

Rocchi, S., Armienti, P., and Di Vincenzo, G. (2005). No plume, no rift magmatism in the West Antarctic Rift. Geological Society of America: 435-437.

Rocchi, S., LeMasurier, W.E., and Di Vincenzo, G. (2006). Oligocene to Holocene erosion and glacial history in Marie Byrd Land, West Antarctica, inferred from exhumation of the Dorrel Rock intrusive complex and from volcano morphologies. Geological Society of America Bulletin 118(7-8): 991-1005.

Saylor, J.E. and Sundell, K.E. (2016). Quantifying comparison of large detrital geochronology data sets. Geosphere 12(1): 203-220.

Siddoway, C.S. and Fanning, C.M. (2009). Paleozoic tectonism on the East Gondwana margin: Evidence from SHRIMP U–Pb zircon geochronology of a migmatite–granite complex in West Antarctica. Tectonophysics 477(3-4): 262-277.

Talarico, F.M. & Sandroni, S. (2009). Provenance signatures of the Antarctic Ice Sheets in the Ross Embayment during the Late Miocene to Early Pliocene: The ANDRILL AND-1B core record. Global and Planetary Change 69(3): 103-123.

Talarico, F.M., McKay, R.M., Powell, R.D.et al. (2010). Late Cenozoic oscillations of Antarctic ice sheets revealed by provenance of basement clasts and grain detrital modes in ANDRILL core AND-1B. Global and Planetary Change 96-97: 23-40.

Tinto, K.J., Padman, L., Siddoway, C.S., et al. (2019). Ross Ice Shelf response to climate driven by the tectonic imprint on seafloor bathymetry. Nature Geoscience 12(6): 441-449.

Triplehorn, D.M., Bohor, B.F., Betterton, W.J. (2002). Chemical Disaggregation of Kaolinitic Claystones (Tonsteins and Flint Clays). Clays and Clay Minerals **50**(6): 766-770.

van Wyk de Vries, M., Bingham, R.G., and Hein, A.S. (2017). A new volcanic province: an inventory of subglacial volcanoes in West Antarctica. Geological Society, London, Special Publications 461(1): 231-248.

Vermeesch, P. (2013). Multi-sample comparison of detrital age distributions. Chemical Geology 341: 140-146.

Vermeesch, P. and Garzanti, E. (2015). Making geological sense of 'Big Data' in sedimentary provenance analysis. Chemical Geology **409**: 20-27.

Yakymchuk, C., Brown, C.R., Brown, M., et al. (2015). Paleozoic evolution of western Marie Byrd Land, Antarctica. Geological Society of America Bulletin 127(9-10): 1464-1484.

Zachos, J.C., Breza, J.R., and Wise, S.W. (1992). Early Oligocene ice-sheet expansion on Antarctica: Stable isotope and sedimentological evidence from Kerguelen Plateau, southern Indian Ocean. Geology 20: 569-573.

Zattin, M., Andreucci, B., Thomson, S.N., et al. (2012). New constraints on the provenance of the ANDRILL AND-2A succession (western Ross Sea, Antarctica) from apatite triple dating. Geochemistry, Geophysics, Geosystems 13(10).

CURRICULUM VITAE

Christopher W. Mallery

Education

June 2022

- Master of Science
- Major: Geology
- Indiana University-Purdue University Indianapolis
- Indianapolis, IN
- Thesis: “The Dynamics of the late Neogene Antarctic Ice Sheets in the central Ross Sea using a multianalytical approach”

May 2018

- Bachelor of Arts
- Major: Geology
- Minor: Geochemistry
- Indiana University-Purdue University Indianapolis
- Indianapolis, IN

December 2014

- Associate of General Studies
- Major: General Studies
- Ivy Tech Community College
- Indianapolis, IN